Oxidation of NO into NO_2 over Activated Carbon Fibers

Isao Mochida*, Seiki Kisamori, Motohiro Hironaka and Shizuo Kawano
Institute of Advanced Material Study, Kyushu University;
6-1 Kasugakoen, Kasuga-shi, Fukuoka 816, Japan.

Catalytic oxidation of NO into NO_2 was studied over activated carbon fibers at room temperature to trap the unreacted NO as well as the oxidized product as the acid or salts.The heattreatment of pitch based activated carbon fiber was found to enhanced markedly the activity to allow the conversion of 82% in dry and 25% in wet air at 25℃ by W/F of 1.0×10^{-2}g · min · ml^{-1}. The strong retardation by humidity on the activity of as-received fiber was moderated by the heattreatedment. The rate of oxidation was examined by varying concentration of NO ,H_2O and NO_2. The catalytic activities of other fibers were also examined in dry and wet air.

Introduction

NO in flue gas or even in the atmosphere has been continuously expected to be removed or converted into unharmful species more extensively and more efficiently. Selective catalytic reducion of NO in flue gases from various sources has been performed in a commercial scale, using vanadium on TiO_2 catalyst in a honey comb from at a temperature range of 300 to 400℃, where the complete decomposition of $(NH_4)_2SO_4$ is achieved.[1] Although such a SCR process appears proven and established, there remain several problems such as a high reaction temperature which requires reheating, large volume of reactor and necessity of reductant ammonia. The process is not applicable to NO from mobile sources or in very low concentration at ambient temperature as observed in urban areas.

Low temperature SCR processes have been explored around 100-150℃ using zeolite and active carbon as the catalysts and ammonia as the reductant.[2] Complete removal of SO_2 before SCR is strictly necessary because $(NH_4)_2SO_4$ tends to plug the reactor as well as the catalyst bed. The present authers have proposed such a process catalyzed by activated carbon fiber (ACF) to reduce NO of 10ppm at room temperature in the atmosphere.[3,4] However, severe retardation by humidity, necessity of ammonia and further activation of ACF with H_2SO_4 may increase the cost to be unceptable .

In the present paper, we describe the catalytic activity of activated carbon fibers and their heattreated ones for the oxidation of NO in flue or air to be captured as the nitric acids or salts. Such an oxidation catalyzed by active carbon has been reported for a long time.[5,6,7] The unsatisfactory activity and strong retardation by humidity so far restricts further development in the practical application.

The present authors have revealed that the surface preperties of activated carbon fiber can be controlled by the selection of precursor, activation conditions and post-modification such as heattreatment as well as chemical treatment. Hence we examined in the present study the catalytic activity of pitch and PAN based activatied fibers and their heattreated ones to explore the high humidity-resistive activity. Very preliminary trials to capture the oxidized nitric species in water and aq bases are also included.

Experimental

Pitch based (OG-5A,-10A,-20A) and PAN-based (PAN-FE300) active carbon fibers (ACFs) were supplied by Osaka Gas and Toho Rayon, respectively in yarn forms.Their propeties are summarized in Table 1.

The fibers were heattreated in N_2 at 200 to 1000℃ for 4h. Properties of the fibers heattreated at 800℃ (H800) are listed also in Table 1. Oxidation of NO was preformed in a fixed bed U-shaped flow type reactor. The weight and length of fiber bed, flow rate, the concentrations of NO in N_2 containing 4-15% O_2, and reaction temperatures were 0.5g, 70mm, 50ml · min^{-1}, 380ppm, and 25-125℃, respectively. Air was humidified at 25℃. Reactant and product gases were analyzed by NOX meter (ECL-77A, YANAGIMOTO Co.,Ltd.).

The Oxidized gas was washed in a washing bottle after the reaction before the analyzer to examine the capture of NO_2 and remaining NO.Water and aq.KOH (1mol/l) were placed in the bottle by the depth of 70mm (100ml).

Results

1. Catalytic activity of a pitch based ACF, OG-5A

Figure 1 illustrates the compositional change of a model gas at the outlet of the reactor at 25℃ over as-received OG-5A. NO in dry air decreased its concentration from 380ppm to 75ppm by passing through the OG-5A for the first 2h and then increased it gradually to 170ppm by 20h. Up to this time, no nitric species except for NO was found in the outlet gas, adsorption of the species being suggested although so far their form is not identified.

At 20h after the gas flow started, NO_2 started to be found in the outlet gas. The concentration of NO_2 steadily increased, while NO both found and missed, being calculated from N balance, decreased. At 40h, the concentrations of NO and NO_2 became stationous to be 100 and 300ppm, respectively, N balance being now obtained. Such staitionary conversions continued at least for 40h.

Increasing humidity in the air decreased the adsorption amount of N species and conversion of NO into NO_2 at the stationary states, shortening the time to reach the stationary state. Although the retardation of humidity was slight when the humidity was below 60%, humidity above 80% retarded very markedly and humidity of 100% decreased severely the NO conversion into NO_2 to

only null.

2. Influence of heattreatment

Figure 2 illustrates the activity of OG-5A heattreated at 800℃ (OG-5A-H800) for the oxidation of NO at 25℃. Although the profile for NO adsorption and oxidation over OG-5A-H800 was similar to that over as-received OG-5A, the activity was certainly much higher by the heattreatment. The stationary conversion of NO into NO_2 in dry air increased to 80 % by the same W/F. The humidity in air reduced the conversion to 87% at 60% r.h., 55% at 80%r.h., 15% at 100%r.h.. Such reduction was certainly much less with the heattreated OG-5A than that with the as-received one. The activity at 80%r.h. should be noted.

Figure 3 summarizes the stationary conversions of NO into NO_2 over OG-5A heatreated at 400 to 1000℃. The heattreatment increased slightly the activity in dry air, providing the largest activity at 800℃. Either lower or higher temperature decreased the conversion. The increase of activity by the heattreatment at 800℃ was most marked when the relative humidity was 80%. Activity increase by four times in comparison with that of as-received OG-5As was very significant. Further higher humidity reduced the conversions over all OG-5A regardless of the heattreatment. Nevertheless OG-5A-H800 exhibited the highest conversion of only 15%. Although the activity increase may be remarkable even under 100%r.h. because the as-received OG-5A exhibited no activity at all under the same conditions.

3. Influences of reaction conditions

Figure 4 summarizes the influences of relative humidity on the conversion of NO over as-received and a heattreated OG-5A-H800 ones. Although the humidity reduced the conversion slightly below 60% but severaly above 60%r.h. especially over 80%r.h., the marked influence of the heattreatment was observed at 80%r.h.. (The activity under 100%r.h. was composed in more detail, varying the W/F.)

The oxygen concentration above 7% provided the same conversion of NO over OG-5A-H800 regardless of relative humidities at 25℃.

Figure 5 illustrates the conversion of NO in a temperature range of 30 to 125℃ over OG-5A-H800 at 4% O_2 in dry and humid airs. Air was humidified at 30℃ to carry 30.4g/m^3 H_2O. Hence, the relative humidity decreased at the higher reaction temperature. The conversion in dry air decreased monotonously with rising the reaction temperature.[5,6] The decrease was marked above 50℃. In contrast, the conversion increased with rising temperature upto 75℃ in the humid air. The conversion decreased above 75℃ as observed in dry air. Higher oxygen concentration of 15% increased more markedly the conversion in humid air at 75℃.

Table 1 summarized the the conversions of NO into NO_2 over PAN, pitch ACFs and their heattreated ones. OG-5A exhibited the largest activity in dry air among the as-received ones. The larger surface areas of pitch ACFs tended to show lower activity. Pitch ACF was more active than PAN-ACF. The heattreatment at 800℃ enhanced the activity of all ACFs, OG-5A-H800 exhibiting the largest activity in dry air. Superiority of pitch ACF was more marked in wet air of 80%, where OG-5A-H800 and PAN-FE-300-H800 exhibited the conversions of 65 and 38%, respectively.

4. Capture of Oxidized NO

Figure 1 illustrates the extent of captured NO_2 and NO at the outlet of the reactor after the catalytic oxidation of NO over OG-5A as-received. Under the conditions described, NO of 380ppm was oxidized into NO_2 by the conversion of 73% as described above. Water in the washing bottle (100ml, depth the of water 70mm.) captured 70% of produced NO_2, passing remaining NO_2 and unreacted NO. Aq.KOH (1mol/l) of 100ml captured all NO_2 produced and 58% of unreacted NO, a removing 91% of NO of the inlet gas. More efficient contact of gas with water or aq.KOH can remove more NO as well as NO_2.

Discussion

The present paper describes the significant catalytic activity of pitch based activated carbon fiber, especially after the heattreatment at 800℃, for the oxidation of NO into NO_2 at 25℃, which is captured rather easily with water or aq. basic solution. Two points may be worthwhile for discussion.

The first point is related to the retardation by humidity as reported in the past[5,6] : The important feature is that the heattreatment improved the resistivity against the humidity, allowing the significant activity at room temperature in air of humidity up to 80%, where the ACF as-received lost the activity very severely.

The hydrophobic surface may be induced on the particular ACF surface of potentially high graphitizability. The removal of oxygen functional groups in forms of CO or CO_2 is well established for the ACF surface.[8] Certain graphitization may be achieved by such a treatment, although the ACF experienced such a temperature in the activation stages. The preference of the pitch based fiber to PAN based fiber is ascribed to the graphitization potential of the former fiber.

Second point is related to the active site for the oxidation on the ACF surface. The heattreatment appears to induce more number or more active sites for the oxidation of NO as well as SO_2 as described in a preceding paper.[9,10] The site is induced by the liberation of CO and CO_2 in contrast to the expectation that the oxidation active site is connected to the oxygen functional group. Unidentified site for oxidation appears to be introduced by the heattreatment. Surface carbon of unsaturation in its valence may be induced.

The interesting point is that PAN and pitch based ACFs exhibited the reverse order of catalytic activity for the oxidation of SO_2 and NO.[11,12]

Different ways of H_2O intervention in the two oxidation reactions may cause the different activity in humid air. The activity in dry air may reflect the different interactions of such substrate with the ACF-surface. Detail characterization of surface is necessary.

In conclusion, the combination of PAN-ACF and pitch ACF after the heattreatment at 800℃ may allow the oxidative removal of both SO_2 and NO at room temperature in their acid forms, providing a base for novel technology for treatment of both flue and atmosphere. The successive application of both ACFs can recover H_2SO_4 and HNO_3, separately.

References

1) M.Grove, W.sturu, Ceram.Eng.Sei.Pore., 1989, *10*, 325.
2) W.Held, A.Konig, T.Richte, L.Puppe, SEApaper, 1990, *13*.
3) I.Mochida, S.Kawano, H.Fujitsu, T.Maeda, Nippon Kagaku Kaishi, 1992, *3*, 275.
4) S.Kawano, S.Kisamori, I.Mochida, H.Fujitsu, T.Maeda, Nippon Kagaku Kaishi, 1993, *6*, 694.
5) O.Kircher, O.A.Hougen, A.I.Ch.E.Jaurnal, 1957, *3*, 331.
6) Chieh CHU, O.A.Hougen, Chem.Eng.Prog., 1961, *57*, 51.
7) M.Iwamoto, N.Mizuno, Catal., 1990, *32*, 462.
8) I.Mochida, S.Kisamori, S.Kawano, H.Fujitsu, Nippon Kagaku Kaishi, 1992, 1429.
9) I.Mochida, T.Hirayama, S.Kisamori, S.Kawano, H.Fujitsu, Langmuir, 1992, *8*, 2290.
10) S.Kisamori, S.Kawano, I.Mochida, Chem.Lett., 1993, 1899.
11) I.Mochida, S.Kawano, S.Kisamori, Prepr.Am.Chem.Soc.Div.Fuel.Chem., 1993, *38*(2), 421.
12) I.Mochida, S.Kawano, S.Kisamori, Prepr.Am.Chem.Soc.Div.Fuel.Chem., 1994.

Table 1 Some Properties of ACFs

ACFs	Ultmate analysis (wt%)						Surface area (m^2/g)	Pore vol. (ml/g)
	C	H	N	O	S	Ash		
OG-5A(As-received)	89.6	1.1	0.7	8.3	tr	0.3	480	0.25
OG-10A(As-received)	91.6	0.9	0.5	6.7	tr	0.3	710	0.37
OG-20A(As-received)	93.9	0.9	0.3	4.6	tr	0.5	1550	0.81
PAN-EF300(As-received)	83.4	0.9	4.7	9.2	0	1.8	875	0.46
OG-5A-H800[a)]	92.1	1.0	0.5	5.8	0	0.6	450	0.23
OG-10A-H800	94.0	0.8	0.4	4.4	0	0.4	620	0.32
OG-20A-H800	95.8	0.6	0.3	2.8	0	0.5	1320	0.68
PAN-FE300-H800	86.9	0.7	3.6	5.8	0	3.0	810	0.42

a) Calcined at 800℃ in N_2

Table 2 Catalytic Activities of ACFs for NO Oxidation in Dry and Humidified Carrier

ACFs	NO conversion (%)		
	r.h.=0%	r.h.=60%	r.h.=80%
OG-5A(As-received)	73	58	18
OG-10A(As-received)	71	56	14
OG-20A(As-received)	64	49	16
PAN-EF300(As-received)	60	43	4
OG-5A-H800	82	74	65
OG-10A-H800	80	71	56
OG-20A-H800	75	66	51
PAN-FE300-H800	71	57	38

NO : 380ppm (N_2 Balance), O_2 : 4.0%
W/F=1×10^{-2} g · min/ml, W=1.0g
Reaction temp. : 25℃
Conversion was observed 40h after the reaction started.

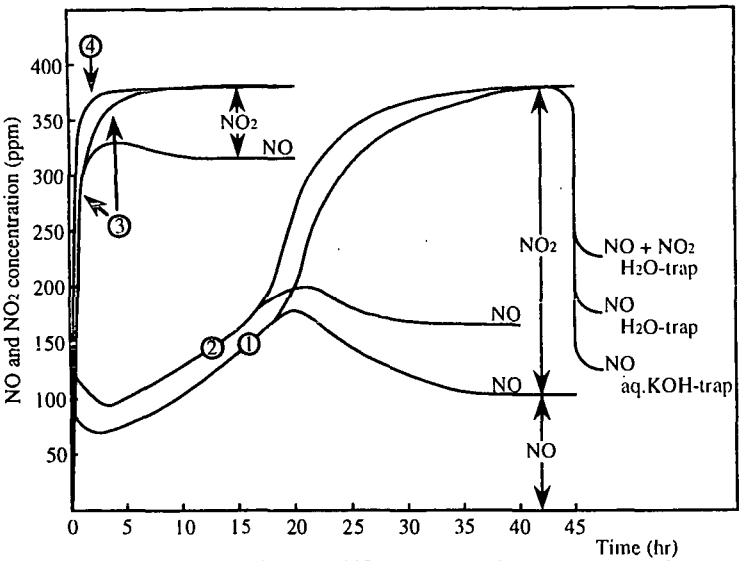

Fig.1 Oxidation of NO into NO_2 over As-received Pitch Based ACF OG-5A

ACF : OG-5A(As-receiced), W=1.0g
NO : 380ppm (N_2 Balance), O_2 : 4.0%
W/F=1×10^{-2}g · min/ml, Reaction temp. : 25℃
Relative humidity : ①0% ②60% ③80% ④100%
Outlet gas passed through washing a botlle.
H_2O : 100ml, depth 70mm, T=25℃
aq.KOH(1mol) : 100ml, depth 70mm, T=25℃

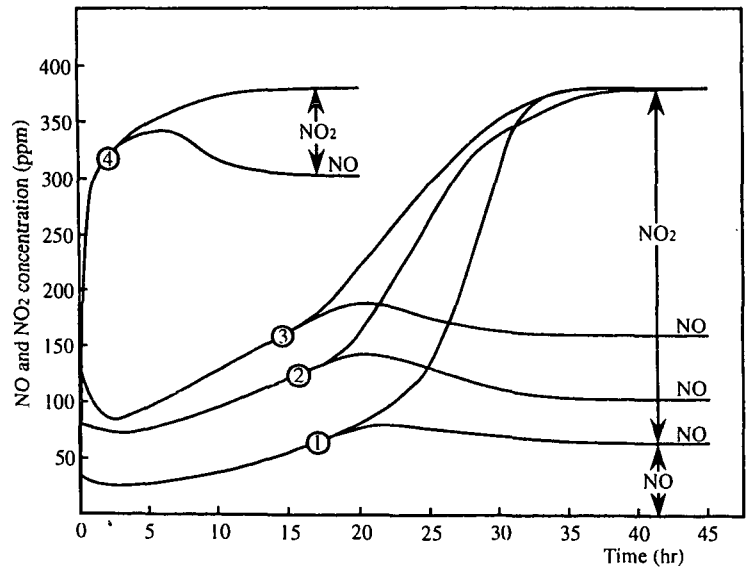

Fig.2 Oxidation of NO into NO_2 over OG-5A Heattreated at 800℃ (OG-5A-H800)

ACF : OG-5A-H800, W=1.0g
NO : 380ppm (N_2 Balance), O_2 : 4.0%
W/F=1×10^{-2}g · min/ml, Reaction temp. : 25℃
Relative humidity : ①0% ②60% ③80% ④100%

A METAL CHELATE PROCESS FOR REMOVAL OF NITRIC OXIDE FROM FLUE GAS

David Littlejohn
Eric K. Pham
S. G. Chang
Energy & Environment Division
Lawrence Berkeley Laboratory
University of California
Berkeley, California 94720

Key words: nitric oxide, flue gas clean-up, metal chelates

INTRODUCTION

Control of sulfur dioxide (SO_2) in flue gases has been achieved by utilization of its high solubility in aqueous solutions. Unlike sulfur dioxide, nitric oxide (NO) has low solubility in aqueous solutions. Consequently, achieving simultaneous control of sulfur dioxide and nitric oxide in flue gas has been difficult to achieve. Nitric oxide can be oxidized to nitrogen dioxide (NO_2), which is more soluble. However, many oxidants are expensive and some of the oxidant material may consumed by the oxidation of dissolved sulfur dioxide. Much of the effort of research for the control of nitric oxide has focused on the development of additives that enhance the solubility of nitric oxide in aqueous solutions. Of the additives investigated, the most promising compounds appear to be metal chelates which are capable of reacting with nitric oxide to form nitrosyl complexes. In particular, many ferrous ion complexes have a high affinity for nitric oxide [1]. Some of the ferrous ion complexes that have been studied have some shortcomings. In particular, ferrous ion-polyaminocarboxylic acid complexes, such as Fe^{2+}(EDTA), are susceptible to oxidation by residual oxygen in the flue gas. The nitrosyl complexes they form react with dissolved sulfur dioxide to form nitrous oxide (N_2O) and nitrogen-sulfur compounds [2]. In recent years, we have investigated thiol-based ligands complexed with ferrous ions that have superior oxidation resistance and NO absorbing capacity [3]. We report here the results of our study of a new thiol-based iron complex using 2,3-dimercapto-1-propane sulfonate (DMPS). It is superior to Fe^{+2}(EDTA) chelate in three aspects: (a) the ability to reduce Fe^{+3} to Fe^{+2}, (b) the absence of nitrogen-sulfur byproducts, and (c) the ease of regeneration using electrochemical reduction. We present here results of the NO removal chemistry of $Fe^{+2}(DMPS)_2$ and the electrochemical regeneration of $Fe^{+2}(DMPS)_2$. Also presented are results of NO thermal desorption studies, which is an alternative regeneration method.

EXPERIMENTAL

NO Absorption Experiments The absorption of NO by $Fe^{+2}(DMPS)_2$ was studied by flowing the gas mixture through a frit at the bottom of a Pyrex column (5cm dia. x 42cm). The $Fe^{+2}(DMPS)_2$ solution was adjusted to pH 5-7 and the temperature of the solution was maintained at 55°C. Simulated flue gas (N_2 with 300-600 ppm NO and 5% O_2) was bubbled through the solution at a flow rate of about 1 L/min, providing a contact time of about 6 seconds. The NO concentration was monitored with a Thermoelectron 14A chemiluminescent NO_x analyzer. The gases were flowed until the NO concentration in the outlet gas matched that of the inlet gas.

Cyclic Voltammetry The electrolytic cell consisted of two flasks separated by an anion-exchange membrane. The cell contained a 0.7 cm dia. glassy carbon working electrode and a platinum foil counter electrode. A saturated calomel electrode was used as reference and 1M Na_2SO_4 was used for the supporting electrolyte. The experiments were performed with a Princeton Applied Research Model 173 potentiostat and a EG&G Model 175 universal programmer. The output was recorded on an XY recorder. All potentials reported are versus SCE.

Electroregeneration of $Fe^{+2}(DMPS)_2$ A somewhat larger electrochemical cell was used for regeneration of the solutions. The cell contained a 11 cm dia. glassy carbon working electrode and a platinum counter electrode separated by an anion exchange membrane. To increase current flow, a barium titanate ultrasonic

transducer was attached to the glassy carbon electrode. During the electroreduction, the solutions in both compartments were agitated with a flow of nitrogen. Under these conditions, the observed current was consistently in the range of 1.5 - 2.0 A for a 0.025 M $Fe^{+2}(DMPS)_2$ solution. Ammonia produced by the reduction was collected in a trap containing 100mL sulfuric acid connected to the electroreduction cell gas outlet. A Dionex 2010i ion chromatograph with a conductivity detector and a CS12 cation column was used to determine the concentration of NH_4^+ in the trap following electroreduction.

Thermal Regeneration of $Fe^{+2}(DMPS)_2$ In these experiments, solutions of 50 mM $Fe^{+2}(DMPS)_2$ were saturated with nitric oxide at 55°C. For thermal desorption, the flow of NO (only) was stopped and the temperature of the $Fe^{2+}(DMPS)_2NO$-containing solution was raised to 95°C. After a fixed amount of time (5 min - 2 h) at 95°C, the solution was cooled down to 55°C. The nitric oxide flow was then restarted to assess the NO removal efficiency of the regenerated solution.

RESULTS AND DISCUSSION

To determine the absorption capacity of $Fe^{+2}(DMPS)_2$ solutions, NO was bubbled through a 10 mM $Fe^{+2}(DMPS)_2$ solution, and the NO absorption capacity was measured with the NO_x analyzer. The NO absorption profile for $Fe^{+2}(DMPS)_2$ exposed to 580 ppm NO at 55°C and pH 6.6 is shown in Figure 1a. By graphically integrating the absorption trace, the amount of NO absorbed was determined, and the concentration of $Fe^{+2}(DMPS)_2NO$ was found to be 7.5 mM in the absence of oxygen. NO absorption under the same conditions except for the addition of 5% oxygen to the gas stream is shown in Figure 1b. It was found that the introduction of 5% O_2 reduces the NO absorption capacity of the solution by 44%. For comparison, a nitric oxide absorption by a 10 mM Fe^{+2}(EDTA) solution under similar conditions is shown in Figure 1c. The solution formed only 2.6 mM of the NO adduct. Introducing 5% O_2 into the gas stream results in a 83% reduction in NO absorption by the Fe^{+2}(EDTA) solution, as shown in Figure 1d. From these measurements, we find that $Fe^{+2}(DMPS)_2$ has 2.5 times larger NO absorption capacity than Fe^{2+}(EDTA) at typical scrubber conditions in the absence of oxygen. Its performance in the presence of oxygen is even better, absorbing 7.5 time more NO than Fe^{+2}(EDTA) in the presence of 5% O_2.

The efficient removal of the NO group from the $Fe^{+2}(DMPS)_2NO$ complex to regenerate $Fe^{+2}(DMPS)_2$ for sustained NO absorption is important in the development of a practical flue gas scrubbing system. Chemical reduction of the coordinated nitric oxide is one such approach that has been used with a number of ferrous nitrosyl complexes. The nitrosyl group of many ferrous ion complexes will react with sulfite ion. However, unlike Fe^{+2}(EDTA)NO and other complexes, the coordinated NO in the $Fe^{+2}(DMPS)_2NO$ complex does not react with SO_3^{2-}/HSO_3^-, even at temperatures up to 95°C. This is advantageous in that no undesirable products such as N_2O and nitrogen-sulfur compounds are formed [2]. At present, no suitable chemical agent has been found to regenerate the $Fe^{+2}(DMPS)_2$ complex due to the relative inertness of the NO group.

In an earlier study, the addition of SH-containing compounds, such as penicillamine, or ß,ß'-dimethylcysteine, had been found to enhance the NO removal ability of ferrous cysteine solutions, resulting in an increase in its NO absorption capacity [4]. However, addition of excess thiolated reagents such as cysteamine, cysteine, or DMPS, showed no notable increase in the NO absorption of $Fe^{+2}(DMPS)_2$. This is illustrated in Figure 2 which shows the effect of excess DMPS on the NO absorption capacity of a 10 mM $Fe^{+2}(DMPS)_2$ solution. There is no appreciable increase in NO absorption beyond a 2:1 complex, $Fe^{+2}(DMPS)_2$.

Since flue gas typically contains 2-8% O_2, it can oxidize Fe^{2+} to Fe^{3+}. DMPS rapidly reduces Fe^{3+} back to Fe^{2+} by electron transfer. However, the resulting oxidation of the SH moiety in DMPS leads to a disulfide (S-S) linkage. To maintain its activity, oxidized DMPS must be reduced to its original form. Electrochemical reduction of the disulfide bond to a thiol has been used to convert cystine to cysteine [5]. We have found that oxidized DMPS can be reduced electrolytically to its original state. Electroreduction can also be used to eliminate the nitrosyl group of the

$Fe^{+2}(DMPS)_2NO$ complex. Cyclic voltammograms of $Fe^{+2}(DMPS)_2NO$ were taken at pH 6 with a scan rate of 50 mV/s using glassy carbon and platinum electrodes. They showed a wave due to the reduction of NO at -0.75 V vs. SCE, in addition to waves associated with the reversible Fe(II)/Fe(III) redox couple. Reduction of S-S linkages has been reported to occur at about -1 V [5], where there is interference from hydrogen evolution with the electrodes. Measurements in our laboratory suggest that the potential that is needed may be somewhat lower.

The fate of the coordinated NO following electroreduction is of interest. Results from our analysis of the reduction products by ion chromatography indicate that the NO is reduced to NH_3 with quantitative yield. There is no evidence, based on gas chromatography analysis, of either N_2 (2-electron reduction) or N_2O (1-electron reduction) being formed. Controlled-potential bulk electrolysis of $Fe^{+2}(DMPS)_2NO$ solutions indicates that current densities of 15-20 mA/cm^2 can be routinely achieved using ultrasound vibration and nitrogen bubbling. Under these conditions, the NO desorption rates, as measured from NO absorption experiments on the electroregenerated $Fe^{+2}(DMPS)_2$ solutions, are 6×10^{-5} mol/min and 1.2×10^{-5} mol/min, in the absence and presence of 5% O_2, respectively. More importantly, there is no attenuation in the NO removal capacity of the electroregenerated $Fe^{+2}(DMPS)_2$ after repeated electroreduction cycles. This indicates that electrolytic decomposition of the chelate is unlikely. Therefore, electrolysis of $Fe^{+2}(DMPS)_2NO$ solutions accomplishes dual tasks in the regeneration of $Fe^{+2}(DMPS)_2$: (1) it electrochemically removes bound NO, and (2) it electroreduces the S-S linkage to reform the S-H groups. This is illustrated in the following scheme:

$$Fe^{+2}(DMPS)_2 + NO = Fe^{+2}(DMPS)_2NO \quad (1)$$

$$Fe^{+2}(DMPS)_2NO + 5H_2O + 5e^- \rightarrow Fe^{+2}(DMPS)_2 + NH_4^+ + 6OH^- \quad (2)$$

$$Fe^{+2}(DMPS)_2 \xrightarrow{O_2} Fe^{+3}(DMPS)_2 \quad (3)$$

$$Fe^{+3}(DMPS)_2 \rightarrow Fe^{+2} + DMPS + \text{oxid. DMPS} + H^+ \quad (4)$$

$$\text{oxid. DMPS} + 2H_2O + 2e^- \rightarrow DMPS + 2OH^- \quad (5)$$

Thermal desorption of NO from $Fe^{+2}(DMPS)_2NO$ represents a simple and attractive method for the regeneration of $Fe^{+2}(DMPS)_2$. We have determined the extent of NO desorption by heating a 50 mM $Fe^{+2}(DMPS)_2$ solution, under anaerobic conditions: the NO-saturated solution containing the resulting 37 mM $Fe^{+2}(DMPS)_2(NO)$ was subjected to several cycles of heating to 100°C for fixed amounts of time followed by NO absorption experiments at 55°C to quantify the amount of NO desorbed. The results are shown in Figure 3 which plots the percentage of $Fe^{+2}(DMPS)_2$ recovered as a function of heating time (from 55°C to 100°C to 55°C). Up to 7.5% of the 37 mM of absorbed NO can be removed by heating the spent solution to 100°C for 2h. Heating times of more than 2h become impractical due to significant water evaporation. There is also no evidence of a linear increase in the amount of NO removed following more than 2h of 100°C heat. These results are reproducible over additional thermal cycles, thus precluding the possibility of thermal decomposition of $Fe^{+2}(DMPS)_2$ and its NO adduct.

In the presence of 5% O_2 and under similar experimental conditions, a 50 mM $Fe^{+2}(DMPS)_2$ solution absorbs 17 mM of NO. Of this amount, only 5% could be desorbed in the presence of 5% O_2 after 2h of heat treatment at 100°C. However, there is a rapid drop off to negligible NO desorption in the second thermal cycle due to the oxidation of DMPS. Thus, to make the process recyclable, electrochemical regeneration of DMPS which is needed to reduce Fe^{+3} to Fe^{+2} for sustained NO absorption must still be used. Even so, a comparison of the NO removal efficiencies in the absence of oxygen clearly indicates that thermal desorption is not as efficient as electroreduction in regenerating $Fe^{+2}(DMPS)_2$.

ACKNOWLEDGEMENTS
This work was supported by the Assistant Secretary for Fossil Energy, U.S. Department of Energy, under contract DE-AC03-76SF00098 through the Pittsburgh Energy Technology Center, Pittsburgh, PA.

REFERENCES

1. Littlejohn, D. and S.G. Chang, Kinetic Study of Ferrous Nitrosyl Complexes. *J. Phys. Chem.*, **1982**. *86*, 537-540.

2. Littlejohn, D. and S.G. Chang, Reaction of Ferrous Nitrosyl Chelates with Sulfite and Bisulfite Ions. *I&EC Res.*, **1990**. *29*, 10-14.

3. Chang, S.G., D. Littlejohn, and D.K. Liu, Use of Ferrous Chelates of SH-Containing Amino Acids and Peptides for Removal fo NO_x and SO_2 from Flue Gases. *I&EC Res.*, **1988**. *27*, 2156-2161.

4. Liu, D.K., L.P. Frick, and S.G. Chang, A Ferrous Cysteine Based Recyclable Process for the Combined Removal of NO_x and SO_2 from Flue Gas. *Environ. Sci. Technol.*, **1988**. *22*, 219-223.

5. Zagal, J.H. and P. Herrera, Electrochemistry of Cysteine and Cystine on Metal-Phthalocyanines Adsorbed on a Graphite Electrode. *Electrochim. Acta*, **1985**. *30*, 449-454.

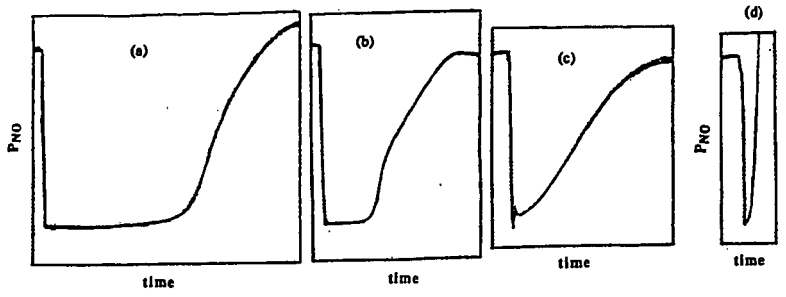

Figure 1. Comparison of NO absorption by $Fe^{+2}(DMPS)_2$ and Fe^{2+}(EDTA) solutions, with and without the presence of 5% oxygen.

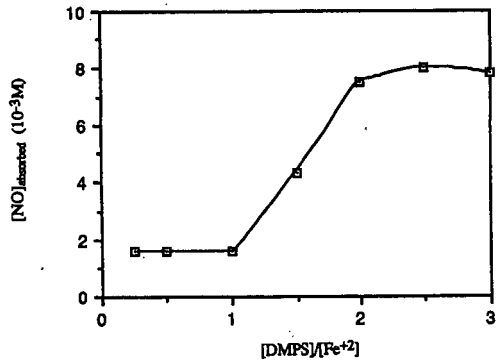

Figure 2. Effect of Fe^{2+}:DMPS ratio on the absorption of nitric oxide.

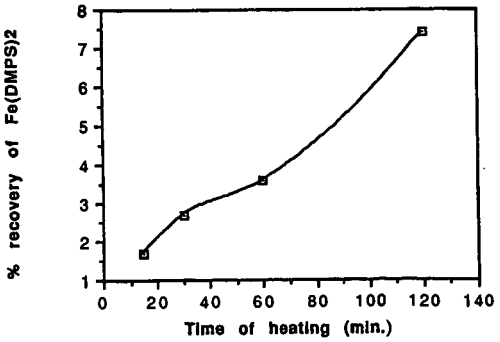

Figure 3. Percent recovery of $Fe^{+2}(DMPS)_2$ as a function of time of heat treatment (55°C –> 100°C –> 55°C) of a 37mM $Fe^{+2}(DMPS)_2(NO)$ solution generated from 50mM $Fe^{+2}(DMPS)_2$ + 550ppm NO (pH 6, 55°C).

SULFUR CAPTURE CAPACITY OF LIMESTONES IN COMBUSTION GASES: EFFECT OF THERMALLY INDUCED CRACKING

Ye Liu, Joel L. Morrison and Alan W. Scaroni
The Pennsylvania State University
402 Academic Activities Building
University Park, PA 16802

Keywords: limestone; thermally induced cracking; sulfation capacity.

INTRODUCTION

Limestones and dolostones can be used in coal-fired, fluidized bed power plants as sorbents to capture SO_2 from the combustion gases. The physical properties of calcined sorbents, especially pore size distributions, and the relationship between these properties and subsequent sulfur capture behavior have been subjects of extensive study[1-4]. In general, calcines of limestones and calcines of dolostones differ not only in chemical composition, but more importantly in physical structure, and this is manifested as a difference in sulfation behavior. Prediction of the development of pore volume and characteristics upon calcination, is usually based on the chemical composition of the starting sorbents[1-3]. These models predict that limestones and dolostones will have different pore structures during and after calcination. They also predict that two limestones or two dolostones with the same chemical compositions will have the same pore structures after calcination.

However, there are numerous examples to show that the pore structures of calcined sorbents differ significantly from those predicted from chemical properties[1,5]. The reasons for this, and the effect this has on sulfation behavior are not well understood.

The work presented here is a study of the sulfur capture capacities of two limestones with high $CaCO_3$ contents (99.4 and 98.5, respectively). The limestones are therefore chemically similar, however, they are petrographically different. Significant differences existed between the physical properties of the calcines and in their sulfation behavior. An explanation for the differences is presented.

EXPERIMENTAL

Two limestones with high $CaCO_3$ contents were collected from different quarries in Pennsylvania (from the Linden Hall and Annville formations). Their physical and chemical properties are given in Table 1.

Calcination and sulfation experiments were conducted in a Perkin-Elmer Series 7 thermogravimatric analyzer (TGA). The reactive gas flow consisted of 15 volume % CO_2, 4% O_2, 2,000 ppm SO_2 and the balance N_2. The flow of 125 standard cubic centimeters per minute (SCCM) was controlled by Brooks Electronic mass flow controllers and was passed downwards over the sample, which was held in a platinum pan of 5 mm diameter. From 4 to 10 mg of sample were used for each run, depending on the particle size. Before starting the rapid heating, the system was thoroughly purged with the reactant gas. To simulate the practical situation in a fluidized bed combustor where sorbent particles are introduced into a high temperature gaseous environment, the samples were heated at the maximum setting of 200 °C/min. to the final temperature of 875°C.

Surface area measurements were performed on an Autosorb-1 gas adsorption system (Quantachrome Corporation) using nitrogen as the adsorbate. The pore size distributions were obtained using an Autoscan mercury porosimeter (Quantachrome Corporation).

Morphological analyses were performed on an EM-30 Environmental Scanning Electron Microscope (ESEM) (ElectroScan). Unlike the traditional SEM, the ESEM is capable of examining specimens without coating. In addition, the examination can be conducted on a hot stage where the specimen can be heated up to 1000° C.

RESULTS AND DISCUSSION

It is generally accepted that at atmospheric pressure and high temperature, it is the CaO formed by the thermal decomposition of $CaCO_3$ that reacts with SO_2 and O_2 according to:

$$CaCO_3 \rightarrow CaO + CO_2 \qquad (1)$$

$$CaO + SO_2 + 1/2\ O_2 \rightarrow CaSO_4 \qquad (2)$$

instead of the direct sulfation of limestone by:

$$CaCO_3 + SO_2 + 1/2\ O_2 \rightarrow CaSO_4 + CO_2 \qquad (3)$$

Figure 1 illustrates typical TGA profiles of the Linden Hall and Annville samples in a simultaneous calcination and sulfation test. The profiles consist of two characteristic portions. At first, the weight loss due to calcination by reaction (1) dominates. Sulfation starts, however, as soon as CaO is formed. This has been confirmed previously by comparing data obtained with and without SO_2 in the calcining gas [6]. During active calcination, the sulfur uptakes were about 5 % (on a S/Ca molar ratio basis) and 10 % for the Linden Hall and Annville samples, respectively, for the particle size of 60x100 mesh. In the second portion of the TGA trace, the sample weight increases with time due to the occurrence of sulfation. The sulfur uptake by reaction (2) is initially rapid, then gradually decreases as pore plugging occurs [7].

Despite similar chemical compositions, for the size fraction of 60x100 mesh, the performance of the Annville sample was much better than that of the Linden Hall sample. This can be related to the larger pore volume in pores greater than 1 μm for the Annville calcine, as shown in Figure 2. Ulerich et al [4] found higher sulfation capacities for calcines with larger pores even though the pore volume and surface area may have been lower than those of calcines with smaller pores. The larger pores facilitate rapid sulfur capture and produce high sulfur capture capacity due to the more rapid transport of SO_2 to the interior of sorbent particles and because the pore plugging effect is minimized [7].

The particle size dependency of the sulfur capture capacity for the Linden Hall and Annville samples is given in Figure 3. The S/Ca molar ratio was calculated from the following equation:

$$\text{S/Ca (molar ratio)} = \frac{[W_i - W_0(1\text{-LOI})] / 80}{W_0\, CaCO_3\% / 100}$$

where:

W_i: Sample weight during sulfation reaction at time t_i,
W_0: Initial sample weight,
LOI: Loss on ignition,
80: Molecular weight of SO_3 (see reaction 2)
100: Molecular weight of $CaCO_3$.

The sulfur capture capacity of the Linden Hall sample increases significantly as the particle size decreases. In a 200 minute run, the S/Ca molar ratio increased from 0.07 for 20x25 mesh particles to 0.47 for 200x270 mesh particles; in comparison, the sulfation performance of the Annville sample had a relatively weak dependence on particle size. As the particle size was changed over the same range, the S/Ca molar ratio only increased from 0.24 to 0.36.

Consequently, for the larger particle size, the Annville sample was superior to the Linden Hall sample, while for the smaller particle size, the opposite was the case. This dependency of performance on particle size is important from a practical viewpoint in that a conclusion that one sample is superior to another based on a test of one particular particle size fraction may not be valid for other particle sizes. In terms of the pore size distributions of the 60x100 mesh particles, it is understandable that for larger particles, the Annville sorbent displayed better performance because of the larger pore volume in larger sized pores. For the Linden Hall sample, the pore plugging effect prevents the interior surface from being accessible to SO_2 and O_2. However, in the case of smaller particles, the above reasoning is not applicable.

The Linden Hall and Annville limestones are chemically similar but geologically different. The Linden Hall is a fine-grained (micritic) limestone and the Annville has undergone recrystallization producing a coarse-grained texture. Their detailed petrographic characterizations are described elsewhere [5]. The petrographic properties of carbonate rocks and their relationship to SO_2 sorption were studied by Harvey and Steinmetz [8,9]. The grain size was found to be an important indicator of sulfation capacity. Among the carbonate rocks tested (including limestone, dolostone, marble and chalk), in general, the finer the grain size of the rock, the higher the sulfation capacity. However, the limestone samples tested exhibited increasing sulfation capacity with increasing grain size [9]. More recently, Zarkanitis and Sotirchos found that fine-grained Greer limestone had a stronger sulfation dependency on particle size than Georgia marble which consisted of coarse calcitic grains [7]. Morrison et al [5] showed using ESEM the occurrence of cracking within the Linden Hall and Annville samples during particle heat up. Extensive cracks developed among the grain boundaries for the Annville sample. For the Linden Hall sample, some particles contained only one or two randomly oriented fractures within the fine-grained structure. The conditions used for these experiments were low pressure (3 torr water vapor) and low heating rate (10 °C/min.).

Figure 4 presents ESEM photographs of Linden Hall and Annville samples, calcined in the TGA in the absence of SO_2. For the Annville sample with larger grains, extensive cracks occurred along the grain boundaries of the 45x60 mesh particles (Figure 4a). As the particle size was decreased to 200x270 mesh, which is of the order of the grain size, there was essentially no fracturing within the grains, as shown in Figure 4b. Few fractures developed in the Linden Hall particles, as typified by the particles shown in Figures 4c and 4d. It should be noted that the surface structure of the calcined Linden Hall particles is much more porous than that of the Annville particles.

The occurrence of cracking in the larger particles of the Annville limestone benefits the sulfur capture process. It also facilitates rapid calcination. Figure 5 shows the ratio of the time to 50% calcination (t_{50}) between the Linden Hall and Annville samples as a function of particle size. For the 200x270 mesh particles (mean size = 63 μm), the calcination rate of the Annville sample is lower than that of the Linden Hall sample. However, for the 60x100 mesh particles (mean size = 193 μm) , the calcination rate of the Annville sample is greater than that of the Linden Hall sample. It is hypothesized that the fractures facilitate the rapid evolution of CO_2 produced by the decomposition of $CaCO_3$, thereby decreasing the CO_2 pressure inside the particle, and this increases the calcination rate.

The importance of the occurrence of fractures within the particles during heat up to the subsequent sulfation behavior is supported by the sulfur distributions within the Linden Hall and Annville particles. The sulfur distribution maps, obtained from a Camera SX50 microprobe, are shown in Figure 6. For the Linden Hall sample, sulfur is concentrated in an outer layer around the particles, while for the Annville sample, sulfur penetrated into the particles and is distributed

along the grain boundaries. Reaction took place at the external surface of the Linden Hall particles, gradually closing the pores and blocking the pathway to the particle interior. This leads to significant intraparticle diffusion effects in the vicinity of the external surface. For the Annville sample, however, SO_2 penetrated into the particle interior through fractures along the grain boundaries and reaction occurred at the external surfaces of grains, which leads to intragrain diffusion effects.

CONCLUSIONS

This investigation examined the dependency of the sulfur capture capacity of two high $CaCO_3$ content limestones on particle size. The extent of sorbent utilization is dependent on the extent of sulfur penetration into the particles or sulfur penetration into the individual grains which comprise a single particle. The occurrence of cracking within particles had a strong impact on the sulfur capture behavior, since it produced significant accessible surface area.

The petrographic properties of sorbents play an important role in determining calcination and sulfation behavior. It has been shown that the cracking pattern is related to grain size, grain-grain interlocking and particle size. The present experiments indicated that cracking occurred between grains rather than within grains, i.e. no cracking occurred in a particle consisting of a single grain. The Annville sample with the larger grains showed a greater cracking tendency. The Linden Hall sample with smaller grains withstood the imposed stress better.

ACKNOWLEDGMENTS:

Financial support for this work was provided by the Pennsylvania Energy Development Authority and the Pennsylvania Aggregates and Concrete Association. Ronald Wincek is thanked for his help in modifying the TGA.

REFERENCES

1 Vogel, G. J., Johnson, I., Lee, S. H., Lenc, J. F., Lescarret, S. A., Montagna, J., Nunes, F. F., Shearer, J. A., Snyder, R. B., Smith, G. W., Swift, W. M., Teats, F. G., Tumer, C. B., Wilson, W. I., Jonke, A. A. *"Supportive Studies in Fluidized Bed Combustion"*, Argonne National Laboratory, ANL/CEN/FE-77-3, Annual Report, July 1976-June 1977.

2 Haji-Sulaiman, M. Z. and Scaroni, A. W. *Fuel*, 1991, **79**, 169

3 Rubiera, F., Fuertes, A. B., Pis, J. J., Artos, V. and Marban, G. *Thermochimica Acta*, 1991, **179**, 125

4 Ulerich, N. H., O'Neill, E. P. and Keairns, D. L. *Thermochimica Acta*, 1978, **26**, 269

5 Morrision, J. L., Liu, Y., Romans, D. E., Pisupati, S. V., Scaroni, A. W. and Miller, S. F. *Proceedings of SO_2 Capture Seminar "Sorbent Option and Considerations"*, National Stone Association, Cincinnati, Ohio, September 19-21,1993

6 Romans, D. E., Liu, Y., Pisupati, S. V. and Scaroni, A. W. *Proceedings of 7th International Conference on Coal Science*, International Energy Agency, Banff, Canada, September 11-17, 1993

7 Zarkanitis, S and Sotirchos, S. V. *AIChE Journal*, 1989, **35**, 821

8 Harvey, R. D. *Environ. Geology Notes, Illinois State Geological Survey*, **38**, 1970

9 Harvey, R. D. and Steinmetz, J. C. *Environ. Geology Notes, Illinois State Geological Survey*, **50**, 1971

TABLE 1 Properties of the Linden Hall and Annville limestones

Limestone	Linden Hall	Annville
BET Surface area (N_2, m^2/g)	0.215	0.155
Porosity (vol. %)	1.0	1.8
Loss on Ignition (wt%)	43.4	43.2
CaO (wt%)	55.7	55.2
MgO (wt%)	0.41	0.54
SiO_2 (wt%)	0.69	0.74
Al_2O_3 (wt%)	0.31	0.35
Fe_2O_3 (wt%)	0.07	0.05
Other minor oxides (wt%)	0.22	0.12
Total (wt%)	100.8	100.2

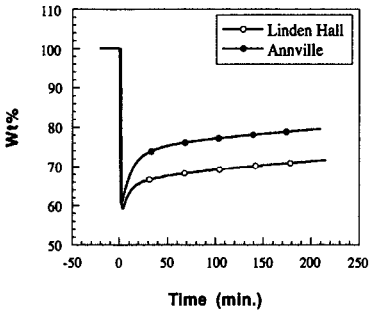

Figure 1 TGA profiles during simultaneous calcination and sulfation of 60x100 mesh sorbent particles

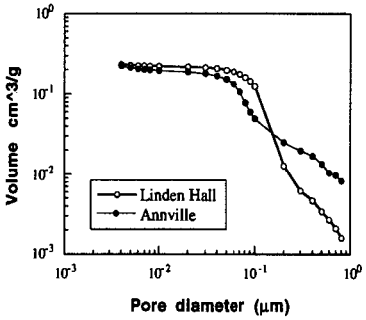

Figure 2 Pore size distributions of calcined 60x100 mesh sorbent particles

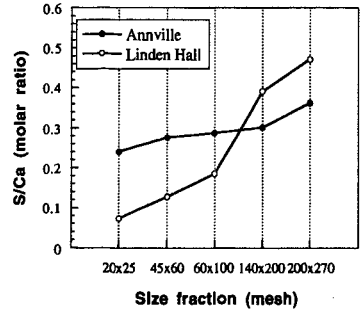

Figure 3 Dependency of sulfur uptake capacity on particle size for a 200 min test

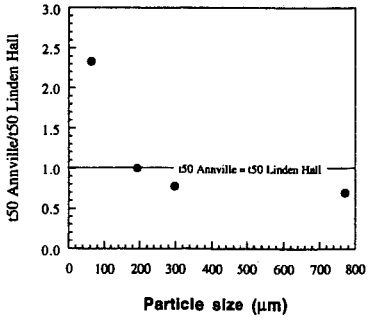

Figure 6 Dependency of the relative calcination time on particle size

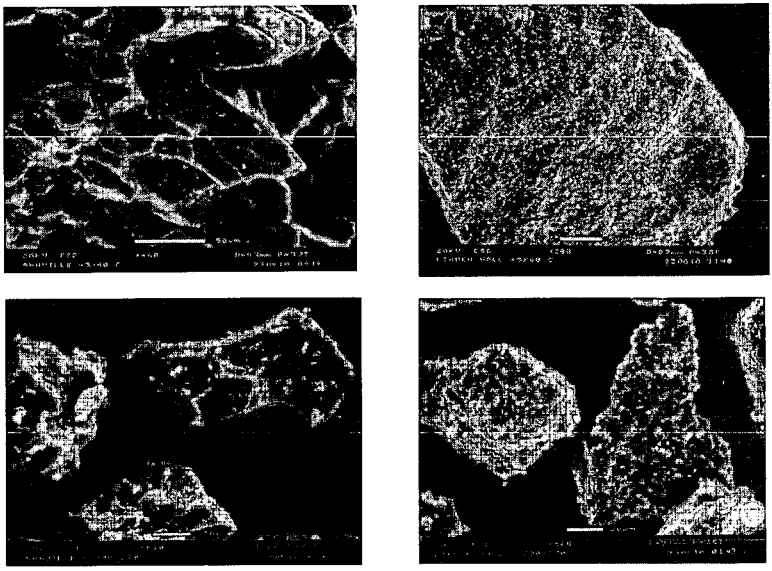

a (above) Annville 45x60 mesh
b (bottom) Annville 200x270 mesh
c (above) Linden Hall 45x60 mesh
d (above) Linden Hall 200x270 mesh

Figure 4 ESEM photographs of calcined Annville and Linden Hall samples

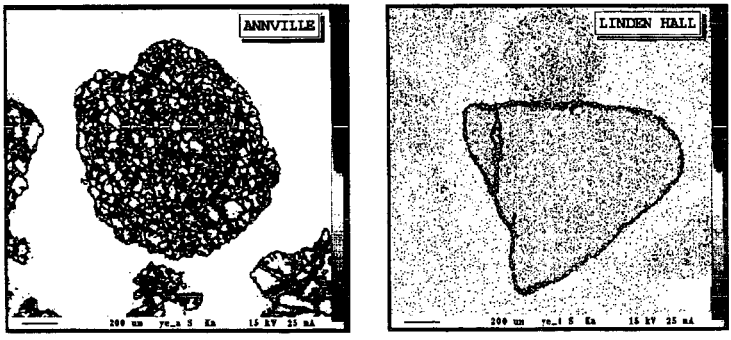

Figure 5 Sulfur distribution maps of sectioned Annville and Linden Hall sulfated particles

EXPERIMENTAL INVESTIGATION OF HIGH-TEMPERATURE, SHORT RESIDENCE-TIME CALCINATION AND SULFATION OF LIMESTONE AND DOLOSTONE SORBENTS

Naiyi Hu, Ye Liu, Sharon Falcone Miller and Alan W. Scaroni
The Pennsylvania State University
402 Academic Activities Building
University Park, PA 16802

Key words: sorbent furnace injection, calcination, sulfation.

INTRODUCTION

Sulfur dioxide emissions from coal-fired utility boilers and furnaces continue to be of significant regulatory concern. One approach to reducing these emissions that has received considerable attention[1-4] is the injection of dry, pulverized sorbent (limestone or dolostone) into the combustion chamber. This technology has been applied to conventional coal-fired utility boilers[1,2] and is considered to be a good candidate for use in coal-fired heat engine applications.[3,4] During the process, the injected limestone or dolostone particles are rapidly heated by the hot combustion gases and calcined by the reactions $CaCO_3 \rightarrow CaO + CO_2$ and $CaMg(CO_3)_2 \rightarrow CaO + MgO + 2CO_2$, respectively. The CaO produced then reacts with SO_2 and excess O_2 in the combustion gases to form $CaSO_4$.

Experimental data on the rates of calcination, sintering and sulfation have been reported by Borgwardt and others.[5-8] The physical structure of the calcined sorbents has also been investigated,[5,9,10] and a number of models have been developed describing the calcination and sulfation processes.[10,11,12] The primary application of dry sorbent injection is to conventional coal-fired utility boilers. The sorbent particle size used is either small (in the range of 1 to 30 μm) in pulverized coal applications or large (in the range of 0.25 to 1 mm) for fluidized-bed applications. Few investigations have been carried out using 30 to 100 μm particles, which is the size range of interest for coal-fired heat engine applications.[3,4]

This study investigated the calcination and sulfation behavior of three different sorbents (two limestones and one dolostone) in the size range from 37 to 105 μm. The time required for heating and calcination, the effect of the calcination process on sulfation behavior, and the effect of sorbent type on sulfation behavior were of primary interest.

EXPERIMENTAL

The calcination and sulfation experiments were conducted in the entrained-flow reactor illustrated in Figure 1. It consists of a preheater, a side-heated sorbent injector, and a vertical reactor. The preheater, injector and reactor were electrically heated to provide the desired gas preheating temperature and reactor temperature. The inside diameter of the ceramic reactor tube is 50.8 mm and it has an isothermal zone length of 600 mm. Dry air was used as the entrainment gas and was preheated to the same temperature as that in the reactor isothermal zone (±13 °C). The total gas flow rate was 60.7 l/min. As the preheated air passes through the injector section, the heat loss caused by contacting the injector wall is compensated for by the heat transferred from the heating wire wound around the outside of the injector. The sorbent was fed by a calibrated fluidized bed feeder. Room temperature air was used for sorbent injection and it comprised 5 % by mass of the total air flow to the reactor. A flow stabilizer was used to eliminate pulsations of the feed material caused by the fluidized feeder. SO_2 was doped into the gas flow by a mass flow controller to provide an SO_2 concentration of 2000 ppmv in the reactor. The sorbent feed rate was adjusted to achieve a Ca/S molar feed ratio of 2.0. Solid samples were collected through a nitrogen-purged, water-cooled sampling probe. During sampling, the nitrogen was used to increase the cooling rate of the sample. The nitrogen comprised 50 % of the total gas flow through the probe. Calculations indicated that 89 μm particles were cooled from 1,100 to 700 °C within 0.03 second after entering the sampling probe.

The stratigraphic formations, chemical compositions and the specific BET surface areas of the two limestone and one dolostone sorbents tested are shown in Table 1. The materials were crushed and wet sieved to size fractions of 74-105 μm (140x200 US mesh), 53-74 μm (200x270 US mesh) and 37-53 μm (270x400 US mesh). The sieved materials were dried in an oven at 105 °C for 48 hours.

The solid samples extracted from the reactor were analyzed for loss-on-ignition (using a Leco MAC-400 proximate analyzer), BET surface area (using a Quantachrome Autosorb-1 analyzer system with nitrogen), and sulfur content (using a Leco SC-132 sulfur analyzer with V_2O_5 catalyst). Some hydration occurred during sample collection and transfer. The extent of hydration was determined (using the Leco MAC-400 proximate analyzer) and the calcination and sulfation data corrected accordingly.

RESULTS AND DISCUSSION

CALCINATION BEHAVIOR

The extents of calcination of the Linden Hall limestone at gas temperatures of 1,000 and 1,100 °C are shown in Figures 2 a and b, respectively. The initial calcination rate is slow, followed by a rapid increase, and then a decline as the calcination process approaches completion.

An initial slow rate of calcination was observed for all three sorbents studied and this was attributed to the use of ambient air as the injecting medium, and the time needed for the sorbent particles to reach their decomposition temperatures.

Effects of Ambient Air Sorbent Injection and Time Required for Particle Heating: Sorbent injection systems typically use ambient air as the injecting medium. To simulate this condition, the sorbents were entrained in air at room temperature. As previously indicated, the sorbent-entraining air comprised 5 %, by mass, of the total air flow to the reactor tube. This ambient air, when mixed with preheated air in the top of the reactor, reduced the reactor inlet temperature. Figure 3 shows the measured gas temperature profiles along the reactor. It was found that the gas temperature, at a location corresponding to 0.1 second after injection, was 40 °C lower than the gas temperature at the same location when no ambient air injection occurred. The lower inlet gas temperature caused by the ambient air injection resulted in a delay in the initial calcination of the sorbents.

Another reason for the significant delay in calcination was the heating time required for the relatively coarse sorbent particles to reach their decomposition temperature. Figure 4 shows the calculated temperature profiles of 10 and 63 μm particles as a consequence of convective heat transfer. It takes much longer for the relatively coarser sorbent particles (in the range of 37 to 105 μm) to heat up than for a 10 μm particle. The characteristic heating time for a 105 μm sorbent particle is 92 ms and that for a 10 μm sorbent particle is only 0.8 ms. This latter time is negligible for conventional utility boilers firing pulverized-coal where the effective sorbent reaction time is about 2 seconds. However, the characteristic heating time for 63 μm sorbent particles is 33 ms, which is significant in heat engine applications.

Effect of Sorbent Particle Size on the Calcination Process: Over the sorbent size range from 45 to 89 μm, the effect of particle size on the calcination process at 1,000 °C is shown in Figures 2 and 5. For the three sorbents studied, the extent of calcination was not significantly dependent on the sorbent particle size.

From the classical shrinking-core model, the extent of calcination can be expressed as:

$$x = 1 - (1 - k \cdot t / dp)^3 \qquad (1)$$

where dp is the particle diameter, k is the calcination rate constant and t is the calcination time. In Equation (1), the extent of calcination has a strong dependency on particle size. Borgwardt[5] demonstrated that, when the resistances of intraparticle and interparticle mass transfer were eliminated, the calcination rate of small limestone particles could be described by a model that assumed a direct relationship with the specific BET surface area of $CaCO_3$. This calcination model has the form:

$$d(CaCO_3) / dt = k \cdot S_g \cdot (CaCO_3) \qquad (2)$$

where $(CaCO_3)$ is the weight of the undecomposed carbonate and S_g is the specific BET surface area of $CaCO_3$. By integration, the extent of calcination is related to the specific BET surface area by:

$$x = 1 - \exp (- k \cdot t / S_g) \qquad (3)$$

Milne et al.[10] employed a modified shrinking-core model to interpret the experimental data of Borgwardt[5]. A good fit was obtained when the particle diameter dependency was reduced to the 0.6 power, and the empirically modified equation was:

$$x = 1 - (1 - k \cdot t / dp^{0.6})^3 \qquad (4)$$

Comparison of the calcination models with the experimental data for the Linden Hall limestone at 1,000 °C is shown in Figure 6. This data indicate that the calcination model based on the specific BET surface area of $CaCO_3$ is a better predictor of the experimental data than the modified shrinking core model. A comparison of the calcination models with the data for the Bossardsville and Nittany sorbents results in the same conclusion.

To be able to apply the modified shrinking-core model to the experimental data of this study requires that the particle size dependency be reduced to a power of between 0.2 to 0.3, depending on the particular sorbent. The very weak particle size dependency implies that these sorbents had very rough surfaces and the different size dependencies of the different sorbents may be related to the physical structures of the sorbents as well as to the chemical reactions that occur on the surface. This issue will be clarified in future studies.

SULFATION BEHAVIOR

The sulfation data for the three sorbents at a gas temperature of 1,000 °C are shown in Figure 7. The extent of sulfation is expressed as the molar ratio of sulfur to calcium in the solid sample. The data reveal that the sulfation process for the limestone and dolostone particles in this size range was different than that associated with small particles (~5 μm) and precalcined sorbents.[13] There were no initial rapid sulfur capture periods as was the case for most small particles and precalcines.[13] The sulfation rates increased steadily and monotonically. In addition, the low calcium dolostone exhibited a greater sulfur capture capability than the high calcium limestone for the same experimental conditions. The 1,100 °C sulfation data for the three sorbents showed the same trends.

Effect of Calcination Rate on Sulfation Rate: Figure 8 shows the calcination and sulfation curves for 45 μm Bossardsville limestone particles at a gas temperature of 1,000 °C. The experimental

data of Cole et al.[13] using precalcined limestone at similar sulfation conditions are also shown in Figure 8 (indicated by the square data points). Comparing the sulfation curves of the 45 μm limestone particles used in this study and that of Cole's study, the initial rapid sulfur capture period, typical of precalcines and small particles, was not apparent. Based on the calcination curves generated in this study, it is concluded that the delay in calcination is responsible for the initial lower extent of sulfur capture. For the 63 μm Bossardsville limestone particles, the extent of calcination was only 8 % for a 0.2 seconds particle residence time. Though the sulfation rate of the CaO produced was very high, there was not sufficient CaO available at that time for extensive sulfation to occur. As a consequence, the sulfur capture (based on the molar ratio of sulfur to calcium) was low. Despite the initial sulfation delay, the slope of the sulfation curve at longer residence times did not level off. The ongoing calcination process produced fresh CaO surface to be sulfated. The production of a $CaSO_4$ layer from the CaO initially produced resulted in a slower rate of sulfation due to product layer diffusion limitations. However, the sulfation rate of newly created CaO was rapid, thereby compensating for the slower rate of sulfation of the CaO beneath the $CaSO_4$ layer. For particle residence times up to one second, which corresponded to an 80 to 90 % extent of calcination, no significant decrease of the apparent sulfation rate was observed.

Effect of Sorbent Type on Sulfation: As shown in Figure 7, the different sorbents exhibited different sulfation performances at the same experimental conditions. For the sulfation tests with 45 μm particles at 1,000 °C and 1.1 second residence time, the calcium utilization of the Linden Hall limestone was 9 %, that of the Bossardsville limestone was 12 %, while that of the Nittany dolostone was 28 %. On the basis of sorbent utilization (rather than calcium utilization), the performance of the lower purity Bossardsville limestone was not significantly different than that of the high purity Linden Hall limestone. The Nittany dolostone, which contained only 50 % calcium carbonate, displayed better performance than the high purity Linden Hall limestone. At a Ca/S molar feed ratio of 2.0, the 45 μm Nittany dolostone particles reduced the SO_2 in combustion gas by 56 % in 1.1 seconds at 1,000 °C.

CONCLUSIONS

1. Simulating the dry sorbent furnace injection process by using ambient temperature air as the injection medium increased the heating time of 37 to 105 μm diameter particles and delayed the calcination process.
2. The extent of calcination was insensitive to particle size in the range studied. The calcination model based on the specific BET surface area of the raw sorbent produced the best fit of the experimental data.
3. The calcination delay significantly affected the apparent sulfation rate for up to 0.2 seconds after sorbent injection. Between 0.2 and 1.0 seconds, the apparent sulfation rate was almost constant.
4. High purity limestones may not be the best choice for use in dry sorbent furnace injection processes. Low calcium dolostone may display better sulfation performance.

ACKNOWLEDGMENTS

Financial support for this work was provided by Manufacturing and Technology Conversion International, Inc. under DOE Contract #DE.AC21-89MC26288. The cooperation of the staff of The Combustion Laboratory is also acknowledged.

REFERENCES

1. Proceedings: *1990 SO_2 Control Symposium,* Session 3A, EPRI GS-6963, Electric Power Research Institute, Sept. 1990
2. Proceedings: *First Combined Flue Gas Desulfurization and Dry SO_2 Control Symposium,* Session 4A, EPRI GS-6307, Electric Power Research Institute, April 1989
3. Abichandani, J. S., *Gas Stream Cleanup Papers from DOE/METC Sponsored Contractors Review Meetings,* DOE/METC-89/6099, Morgantown, WV, 1988, p.167
4. Lawson, W. F., Maloney, D. J., Shaw, D. W. Richards, G. A., Anderson, R. J., Cook, J. M., Siriwardane, R. V., Poston, J. A. and Colaluca, M. A., *Proceedings of Seventh Annual Coal-fueled Heat Engines and Gas Stream Cleanup Systems Contractors Review Meeting,* DOE/METC-90/6110, Morgantown, WV, 1990, p.283
5. Borgwardt, R. H., *AIChE J.*, 1985, **31**, 103
6. Borgwardt, R. H. and Bruce, K. R, *AIChE J.*, 1986, **32**, 239
7. Borgwardt, R. H., Roache, N. F. and Bruce, K. R., *Ind. Eng. Chem. Fundam.*, 1986, **25**, 165
8. Powell, E. K. and Searcy, A. W., *Metallurgical Trans.*, 1980, **11B**, 427
9. Newton, G. H., Chen, S. L. and Kramlich, J. C., *AIChE J.*, 1989, **35**, 988
10. Milne, C. R., Silcox, G. D. and Pershing, D. W., *Ind. Eng. Chem. Res.*, 1990, **29**, 139
11. Milne, C. R., Silcox, G. D. and Pershing, D. W., *Ind. Eng. Chem. Res.*, 1990, **29**, 2201
12. Dam-Johansen, K., Hansen, P. F. B. and Østergaard, K.,*Chem. Eng. Sci.* 1991, **46**, 847
13. Cole, J. A., Kramlich, J. C., Seeker, W. R., Silcox, G. D., Newton, D. W., Harrison, D. J. and Pershing, D. W., Proceedings: *1986 Joint Symposium on Dry SO_2 and Simultaneous SO_2/NO_x Control Technologies,* Vol. 1, 16-1, EPRI CS-4966, Electric Power Research Institute, Dec. 1986

Table 1. Stratigraphic formations, chemical compositions and BET surface areas of the sorbents

Formation	$CaCO_3$	$MgCO_3$	SiO_2	Al_2O_3	Fe_2O_3	BET surface area (m^2/g)		
						45μm	63μm	89μm
Linden Hall	99.42	0.86	0.69	0.31	0.07	0.422	0.396	0.351
Bossardsville	86.93	1.91	8.07	1.46	0.95	0.648	0.613	0.579
Nittany	49.62	39.30	8.01	1.41	0.53	0.534	0.477	0.376

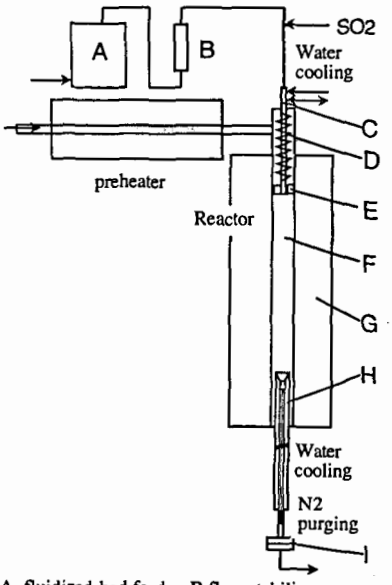

A fluidized-bed feeder, B flow stabilizer
C sorbent and SO2 injector
D injector outside heating
E flow straightener, F reactor tube
G electric furnace, H solid sampling probe
I sample filter

Fig. 1 Schematic diagram of entrained-flow reactor

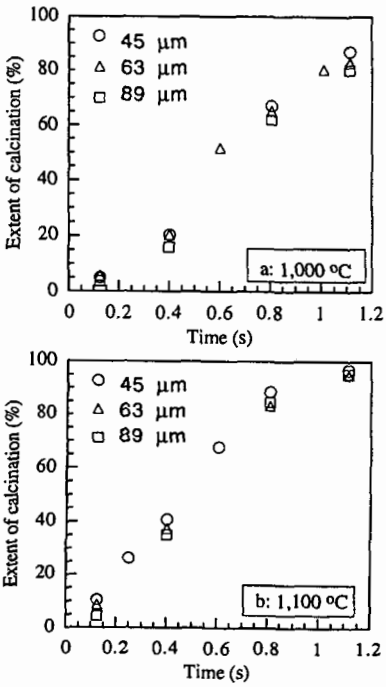

Fig. 2 Time dependency of the extent of calcination of the Linden Hall limestone at a) 1,000°C and b) 1,100°C for various particle sizes

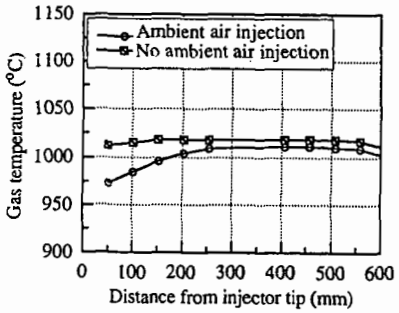

Fig. 3 Effect of injecting sorbent with ambient air on the gas temperature profile along the reactor

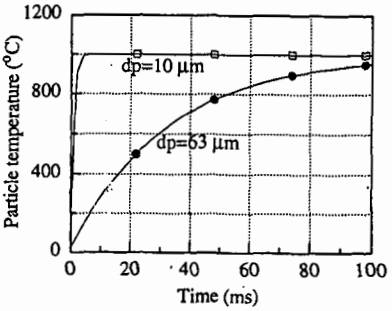

Fig. 4 Calculated sorbent particle temperature profiles during convective heating for 10 and 63 μm particles

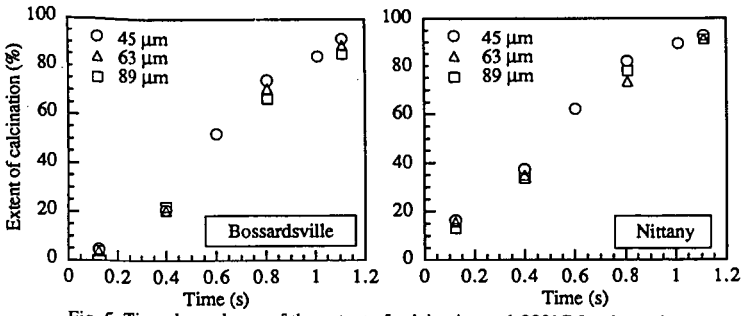

Fig. 5 Time dependency of the extent of calcination at 1,000°C for the various particle sizes of the Bossardsville and Nittany sorbents

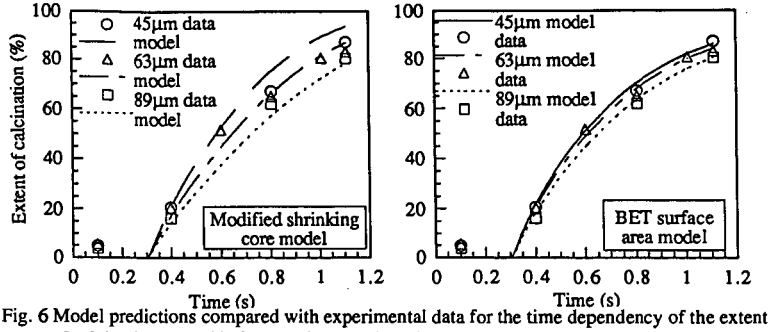

Fig. 6 Model predictions compared with experimental data for the time dependency of the extent of calcination at 1,000°C for various particle sizes of the Linden Hall limestone

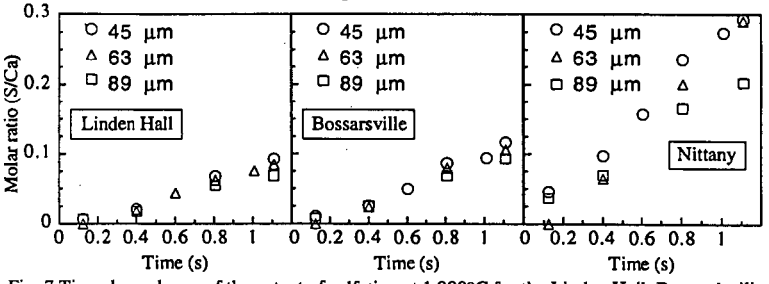

Fig. 7 Time dependency of the extent of sulfation at 1,000°C for the Linden Hall, Bossardsville and Nittany sorbents

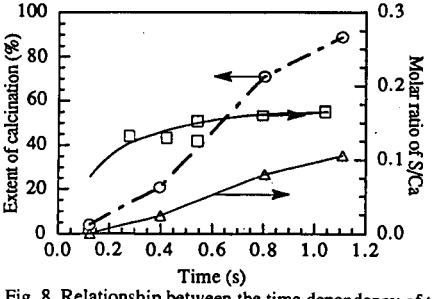

Fig. 8 Relationship between the time dependency of the extents of calcination and sulfation at 1,000°C of 63 μm Bossardsville limestone particles

MODIFIED PEROVSKITES, $La_{1-x}Mg_xMO_3$, - EXCELLENT De-SOx AGENTS.

Jin S. Yoo, C. A. Radlowski, and J. A. Karch*, Amoco Research Center, P.O. Box 3011, Naperville, IL 60566, *UOP, 25 E. Algonquin Road, Des Plaines, IL 60017-5017

Keywords: $DeSO_x$, modified perovskites, FCC regenerator

INTRODUCTION

The De-SO_x catalyst, cerium containing mixed spinel materials, $Ce/MgO \cdot MgAl_{2-x}M_xO_4$ M=Fe, V, Cr, Mn etc) has been effective for the SO_x and NO_x removal from the emission of the fluid catalytic cracking (FCC) regenerator [1,2]. Another type of mixed metal oxides structurally analogous to the naturally occurring mineral perovskite ($CaTiO_3$) have for decades formed the testing and breeding ground for ideas in solid state chemistry. The properties of perovskites that are important in catalysis are primarily the stability of mixed valence states of Co, Mn, Ti, etc., the stabilization of unusual oxidation states, and in particular, the mobility of oxygen ions.

For the automotive application, encouraging results were obtained with manganite and cobaltate perovskites in the oxidation of CO and the reduction of NO. The sensitivity of these particular perovskites to deactivation by SO_2 dampened the initial enthusiasm for their application in automotive exhaust catalysis. Since then, the deactivation mechanism has been understood, the SO_2 resistant catalysts such as $La_{0.6}Sr_{0.4}Co_{1-x}M_xO_3$ has been found [3]. IR spectroscopy indicates that SO_2 absorbed on B sites ions in perovskite, AB_3, deactivate the catalyst by blocking the surface sites that are necessary for CO absorption and lattice oxygen replenishment. The poisoning is due to the stable sulfate formation on B sites with SO_3 formed by oxidation of SO_2 in O_2 [4]. This prompted us to look into application of these types of mixed oxides materials for SO_x removal from the emission of FCC regenerator.

EXPERIMENTAL

Catalyst preparation - over recent years specialized catalyst preparation techniques such as freeze-drying and various types of sol-gel process have been used to produce oxides in a fine partiuclate form. In particular the amorphous citrate process [5] and chemical vapor deposition technique [6] have been shown to be effective because of the high yields of uniformly dispersed mixed oxides with high surface area. However, the modified perovskites studied in this work were prepared by the coprecipitation method for simplicity. The preparation of modified perovskites is described using $La_{0.5}Mg_{0.2}CoO_3$ as an example. The catalyst was precipitated from the aqueous nitrate solutions of La, Mg, and Co with n-butylamine according to the procedure discussed in a previous paper [7]. These nitrates of La, Mg, and Co were dissolved in the minimum amount of water. The pH of aqueous solution of La, Mg, and Co were 0.50, 4.75, and 0.76, respectively. These three metal nitrate solutions were mixed with agitation, and the n-butylamine was added dropwise to produce a coprecipitate over an hour. A spectacular color change and an exothermicity were observed. After amine addition was complete, the slurry pH was 9.46, and the pH of the mother liquor was 9.64. The final slurry was extremely viscous and required vigorous stirring. The slurry was filtered, a water wash followed by an ethanol wash to remove final trace of n-butylamine. The resulting cake was allowed to dry in air and further dried in a vacuum oven at 100°C for 12 hours. The dried cake was a crumbly multi-colored solid. The solid was a uniform color after grinding to 40 minus mesh. The 40 minus mesh grind size was fluidized while cartying out calcination at 732°C for 3 hours. The empirical formular of the final dark-brown product was $La_{0.5}Mg_{0.2}CoO_3$.

The SO_x pickup half cycle - Absorption of SO_3 on the catalyst was measured on an Omni Thermal Analysis System which employs a model 35000 Data Reduction system and a rebuilt Du pont 951 Thermogravimetric Analyzer (TGA). The TGA analyzer was equipped with a special reaction cell to allow the use of corrosive gases (i.e. SO_2) without affecting the delicate balance mechanism. The following test procedure was followed: 1) Approximately 8 mg of catalyst was placed on a quartz pan on the TGA balance. 2) The reaction cell was connected to gas lines and exhaust line. Purged with nitrogen at a flow rate of 200 cc/min throughout an entire run to sweep reacting gases away from balance and out exhaust line. 3) Nitrogen was passed at 100 cc/min while sample was heated at 25°/min to 732°C. 4) After the reactor temperature stabilized at 732°C, the N_2 gas was shut off and the gas blend containing 1.5% SO_2 and 5.9% O_2 in N_2 was introduced over the sample at 100 cc/min. 5) Maintained a weight gain for 15 min while the data point was taken every 10 seconds. 6) At the end of 15 min, the reactor was allowed to cool down, shut off the SO_2 blend gas and switched to air (100 cc/min) for 5 min. When the reactor was cooled to 500°C, air was switched to N_2. It was assumed that a net weight gain was attributed to the SO_3 uptake, and % sulfur was calculated from the net weight gain.

The H_2 reduction half cycle - The sulfated sample resulting from the SO_x pick-up half cycle was reduced with H_2. 1) The sulfated sample was heated to 677°C (in some cases 677 – 732°C) under the N_2 flow of 100 cc/min at a rate of 25°C/min. 2) After the

temperature was stabilized, N_2 is shut off and H_2 was admitted at a rate of 100 cc/min. A weight loss was monitored for 10 min (data points were taken every 2 seconds). 3) At the end of 10 min., the oven was shut off, H_2 was shut off and then N_2 was admitted at 100 cc/min. A catalyst cycle was complete by conducting the SO_x pick-up half cycle and then the H_2 reduction half cycle in sequence. The catalyst stability was determined by the prolonged catalyst cycle tests.

RESULTS AND DISCUSSTIONS

The oxidative SO_x pick-up half cycle - A series of modified perovskite type mixed oxides, $La_{1-x}Mg_xMO_3$, where M=Mn, Co, Cu, Fe were prepared by the coprecipitation procedure. The evaluation of the calcined materials was conducted according to the procedure described in the experimental section. A feed consisting of 1.5% SO_2, 5.9% O_2 and the balance N_2 passed over the catalyst on a pan in the cell of du pont 951 Thermogravimetric Analyzer for 15 min at 732°C. The typical results for manganite, cobaltate, ferrate and cuprate are compared in Figure 1.

H_2 reduction half cycle - The sulfated manganite such as $MgMnO_3$ and $La_{0.2}Mg_{0.8}MnO_3$ and modified cobaltate such as $La_{0.8}Mg_{0.2}CoO_3$ and $La_{0.5}Mg_{0.5}CoO_3$ in the SO_x pick-up half cycle was subjected to the H_2 reduction half cycle. After the catalyst blend in a FCC equilibrium catalyst was sulfated in the SO_x pick-up half cycle, the sulfated system was flushed with nitrogen, brought back to 677°C, reduced in flowing H_2 for 5 minutes, flushed with N_2, and then retested for the SO_x pick-up reaction. The catalytic cycle, SO_x pick-up half cycle followed by H_2 reduction half cycle, was repeated with these catalysts. The weight change (mg) occurred in each half cycle was presented along with calculated S% on the catalyst in Table 1, and plotted in Figure 2. Among these catalyst, $La_{0.8}Mg_{0.2}CoO_3$ appears to be the most stable and promising one.

It has been well known that perovskites are able to exchange oxygen quite easily as the oxidation state of the metals changes due to oxidation or reduction. Reller and colleagues [8] have shown the following conversion: $CaMn^{+4}O_3 \rightleftharpoons CaMn^{+2}O_2 + H_2O$ under H_2 at 500-600°C. It is thus difficult to measure the reduction capability of a sulfated perovskites by TGA. The reaction we want to observe is: $M\text{-}O\text{-}SO_3 + H_2 \rightarrow M\text{-}O + H_2 + SO_2$, where the weight loss is solely due to the loss of SO_3. But the abstraction of labile oxygens from the perovskite lattice complicates the interpretation of the weight loss observed. This phenomenon has been observed in reductions of the sulfated peroskites. The final weight after reduction is lower than the initial weight of the sample (before sulfation) in our own work as well. Any pickups occurred subsequent to the reduction will not only indicate the weight gain of SO_3 but also the replacement of any oxygen missing from the lattice. Because the TGA indicates only weight losses and gains, one must report to final testing of the perovskite catalysts in a cyclic unit where actual pick-up of SO_2 after the sulfate reduction step can be monitored. This will indicate whether or not sulfur is being removed by the reduction or picked up on the catalyst.

Non-oxidative SO_x pick-up chemistry

The same modified cobaltate, manganite, and ferrate were also subjected to non-oxidative SO_x uptake in a feed containing 1600 ppm SO_2 in N_2 by varying the reaction temperatures. The results shown in Table 2 indicate that some of the samples were excellent for SO_x uptake. Catalyst D, $La_{0.8}Mg_{0.2}CoO_3$, exhibited the highest activity in the non-oxidative system among the catalysts studied. Figure 3 is a plot of non-oxidative SO_x pick-up as a function of temperature. Main reactions occurring in the non-oxidative system are believed to be disproportionation of metal sulfite, MSO_3, into sulfate and sulfide [9], and direct reduction of SO_2 to elemental sulfur by the reducing agent such as CO [10]. These results suggest that modified perovskites can be used either in oxygen rich or in oxygen starved FCC regeneration mode.

CONCLUSIONS

A series of modified perovskites, $La_{1-x}Mg_xMO_3$, where M=Co, Mn, Cu, Fe, x=0-1, was found to be effective for removing SO_x from the emission of the fluid catalytic cracking regenerator. Typical modified perovskite samples such as $La_{0.2}Mg_{0.8}MnO_3$, $La_{0.8}Mg_{0.2}CoO_3$, $La_{0.5}Mg_{0.5}CoO_3$, and $La_{0.8}Mg_{0.2}FeO_3$ were prepared by the coprecipitation method. These materials were evaluated for the SO_x removal activity in the two types of feed streams containing 1.5% SO_2 in N_2 with or without 5.9% oxygen. These samples exhibited a remarkable SOx absorption activity in both streams. The catalyst stability of $La_{0.8}Mg_{0.2}CoO_3$ was demonstrated with the catalyst cycle test in an automated laboratory reactor. It is encouraging to find that these materials are also very active under the non-oxidative stream. This suggests that these materials can be used either in the oxygen rich or in oxygen starved FCC regeneration modes.

REFERENCES

1. J. S. Yoo, A. A. Bhattacharyya, C. A. Radlowski, and J. A. Karch, Appl. Catal. B: Environmental, 1 (1992) 169.
2. J. S. Yoo, A. A. Bhattacharyya, and C. A. Radlowski, I&EC Res., 30 (1991) 1444.
3. W. Li, Q. Hwang, W. Zhang, B. Lin, and G. Lee, Stud. Surf. Sci. Catal., 30 (1987) 405.
4. M. Yu. Sultanov, I. S. Al'tsshel, and Z. Z. Makhmudova, Kinet. Katal., 28(1) (1987) 236.
5. H. Zhang, Y. Teraoka, and N. Yamazoe, Chem. Lett., (1987) 665: M. S. G. Baythoun and F. R. Sale, J. Mater. Sci., 17 (1982) 2757.
6. J. S. Yoo, J. A. Donohue, M. S. Kleefisch, P. S. Lin and S. D. Elfline, Appl. Catal. A: General 105 (1993) 83.
7. T. Nakamura, M. Misono, T. Uchijima, Y. Yoneda, Nippon Kagaku Kaishe, No.11 (1980) 1680.
8. A. Reller, G. Davoodabady, H. Oswald, Thermochimica Acta, 83 (1985) 121.
9. C. Castelliani, Gass Chim. Ital., 93(10) (1963) 1252; 93(11) (1963) 1444; 92 (1962) 447; 91 (1961) 173.
10. D. B. Hibbert and R. H. Campbell, Appl. Catal., 41 (1988) 273.

Table 1

The catalytic cycle test, SO_x pick-up half cycle and sulfate reduction half cycle
Catalyst: A:$MgMnO_3$, B:$La_{0.2}Mg_{0.8}MnO_3$, C:$La_{0.5}Mg_{0.5}CoO_3$. D:$La_{0.8}Mg_{0.2}CoO3$,
Surface area. m^2/g: C:22, D:1

	S pick-up, mg				S removed, mg				S% on catalyst			
Catalyst	A	B	C	D	A	B	C	D	A	B	C	D
# of cycle												
1	49	46	46	35	34	18	29	13	13.0	12.4	12.4	10.2
2	33	14	32	17	26	13	31	17	13.4	12.2	13.5	11.5
3	23	9	30	14	23	9.6	30	12	12.8	11.4	13.5	10.9
4	18	7	26	15	19	8.6	27	13	11.8	10.8	12.8	11.4
5	16	8	24	14	20	8.3	-	-	11.2	10.7	12.2	11.2
6	18				18				10.7			

Table 2

The SO_x pick-up test in a non-oxidative system
2% blend of catalysts in an FCC equilibrium catalyst
Catalyst D: $La_{0.8}Mg_{0.2}$ CoO_3, E:$La_{0.2}Mg_{0.2}MnO_3$, F:$La_{0.8}Mg_{0.2}FeO_3$

Catalyst	% SO_x picked up					Activity	
Temp. °F	500	800	1000	1200	1350	1200	1350
D	12	16	31	63		28	
E					52		22
F					36		14

Fig. 1. Comparison of oxidative SOx pick-up results - S% vs time
La.5Mg.5MO3, M = Mn, Co, Fe, Cu

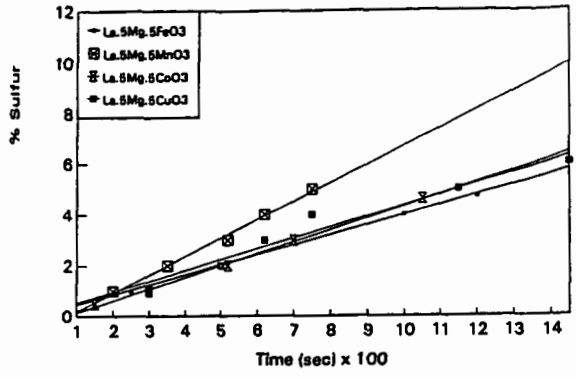

Fig. 2. The stability study of modified perovskites - SOx activity vs catalyst cyle
Repeating a catalyst cycle, SOx pickup half cycle followed by H2 reduction half cycle

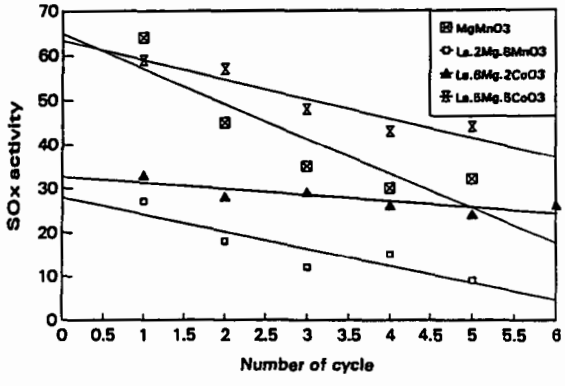

Fig. 3. Non-oxidative SOx pick-up of modified perovskite
SOx pick-up vs temperature, 1600 ppm SO2 in N2

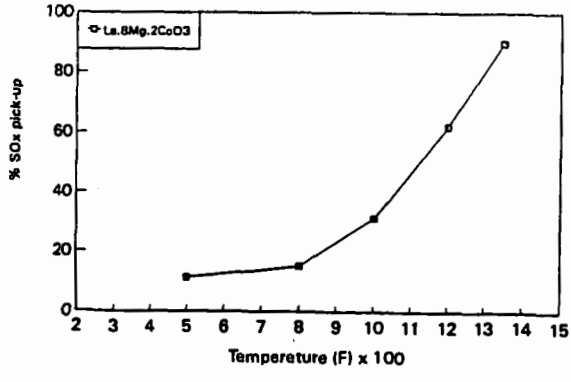

Oxidative Removal of SO_2 and Recovery of H_2SO_4 over Polyacrylonitrile-Based Active Carbon Fiber

S. Kisamori, K. Kuroda, S. Kawano, and I. Mochida
Institute of Advanced Material Study, Kyushu University,
6-1 Kasuga-koen, Kasuga, Fukuoka 816

Keywords : SO_2 removal, SO_2 Oxidation, Activated Carbon Fiber

Abstract

SO_2 was adsorbed, oxidized, hydrated, and recovered continuously as aq. H_2SO_4 at 30-100℃ on a polyacrylonitrile based active carbon fiber (PAN-ACF-FE-300). SO_2 of 1000 ppm in a model flue gas was removed completely for longer than 60 h at 30 and 50℃ by W/F=5.0×10^{-3} g min ml^{-1} by supplying sufficient humidity of 10 and 20 vol%, respectively. The heat-treatment of the ACF at 800℃ was found very effective to enhance the catalytic activity, the temperature appearing very best between 30 to 1000℃. A pitch based activated carbon fiber exhibited less activity than PAN-ACF.

Introduction

More energy-saving, deeper removal of SO_2 in the flue gas has been expected to be developed for the better environment with smaller increase of the cost. Although the wet desulfurization of flue gas using calcium hydroxide in water has been widely commercialized[1], desulfurization of higher efficiency is expected. The conventional desulfurization consumes calcium hydride, to produce gypsum of low value as by-product, or solid waste, requiring a large amount of water and leaking ca. 50 ppm of SO_2. Oxidative adsorption of SO_2 in the form of H_2SO_4 on active carbon or coke around 130℃ is a basis for a dry process[2-4]. The present authors have reported a remarkably large capacity of PAN-ACF among various ACFs for such an oxidative adsorption[5,6]. Such a dry process using carbon adsorbents should heat up the adsorbents after the SO_2 adsorption to recover SO_2 adsorbed in the form of H_2SO_4 on the carbon surface and to regenerate the adsorption ability. At the same time, oxygen functional groups which are introduced by adsorption and desorption of SO_2 should be removed because such oxygen functional groups reduce SO_2 adsorption ability of ACF[7,8]. The reduction of SO_3 into SO_2 at the recovery consumes the carbon as carbon dioxide or monoxide. The carbon adsorbent loses its weight and adsorption ability very rapidly, when flue gas of large SO_2 concentration is charged. Such energy and carbon consumption is one of the critical disadvantages[2,7]. Hitachi has proposed extraction of adsorbed SO_2 on active carbon with water, however, it took so much water to obtain a diluted H_2SO_4[9].

The present paper proposes a solution of the problems, by recovering aq. H_2SO_4 continuously from the surface of PAN-ACF at the SO_2 removal temperature without any carbon loss. PAN-ACF is certainly active to oxidize catalytically SO_2 into SO_3 even at room temperature. Hence continuous hydration of SO_3 may allow the flow of aq. H_2SO_4 from the ACF surface to the reservoir, liberating the active sites to continue the oxidation and hydration of the successive SO_2 molecule. The present process can be applicable to remove SO_2 in the atmosphere as well as flue gas without any difficulty.

Experimental

FE series of PAN-ACFs were supplied by Toho Rayon Co. OG series of pitch ACFs were supplied by Osaka gas. They were heat-treated in nitrogen at 30 to 1000℃. Some of them properties are summarized in Table 1.

SO_2 removal was carried out at 30-100℃ using a fixed bed flow reactor which is illustrated in Fig.1. A model flue gas containing SO_2 of 1000 ppm, O_2 of 5 vol% and H_2O of 10-30 vol% in nitrogen was used. H_2SO_4 was trapped at the outlet of the reactor as illustrated in Fig.1. A part of H_2O was condensed to dew drops in the reactor when water vapor of 10 and 20 vol% was introduced at 30 and 50℃, respectively. Therefore, concentrations of SO_2 and O_2 in the model gas were increased slightly and the total flow rate was decreased slightly in these cases compared

with other cases. SO_2 concentrations in inlet and outlet gases were observed continuously by a frame photometric detector (FPD). Weights of ACF examined and the total flow rate were 0.25, 0.5, and 1.0 g, and 100 ml min^{-1}, respectively.

Results

Figure 2 illustrates the break-through profiles of SO_2 at 30℃ through the beds of two PAN-ACFs and three pitch ACFs of all as-received forms. The gas carried 10 vol% water in all cases. Over PAN-ACF FE-300 which exhibited the largest adsorption capacity, SO_2 was adsorbed completely until 1.6 h (the break-through time T_0), no SO_2 being detected at all at the outlet of the reactor and then SO_2 started to leak concentration increasing rather gradually to 15% of the inlet SO_2 after 5 h. The concentration was kept at this level for at least 13 h, major SO_2 of 80% was removed continuously from the flowing gas.

Other ACFs exhibited similar profile of SO_2 adsorption and removal, although the T_0 and the level of SO_2 stationary concentration were dependent on ACFs. The levels of the stationary concentration were 18% over PAN-ACF-FE 300, 22% over FE-100, 38% over OG-5A and OG-20A, and 45% over OG-10A. The higher activity of PAN-ACF for SO_2 removal was definite. The value of T_0 ranged 0.5 to 18 h, PAN-ACF exhibiting slightly longer break-through time.

Figure 3 illustrates effects of heat-treatment on break-through profiles over PAN-ACF-FE-200 and FE-300 at 30℃, 10 vol% of H_2O. The heat-treatment was very effective to decrease the level of SO_2 stationary concentration as well as to prolong the break-through time as reported before[11]. A particular temperature of 800℃ was found most favorable for both FE-200 and FE-300. The complete removal of SO_2 by both ACFs continued for in least 60 h at 25℃ by W/F of 5.0×10^{-3}g min ml^{-1}. Further higher temperature reduceed the activity.

Figure 4 illustrates the break-through profiles of SO_2 at several temperatures through the bed of FE-300-800. SO_2 was adsorbed completely at 100℃ until 5.1 h, no SO_2 being detected at all at the outlet of the reactor, and then SO_2 started to leak, its concentration increasing rather rapidly to 100% of the inlet SO_2 after 10.5 h. SO_2 of 4.0 mmol g^{-1} was captured on the ACF at 100℃. Lower temperature of 80℃ extended the break-through time to 8.5 h until SO_2 was detected at the outlet of the reactor. After the break-through, SO_2 concentration at the outlet increased rather gradually by 24 h until it reached to 65% of the inlet concentration, and that of the outlet stayed at the same level later on until at least 45 h. Further lower temperature of 50℃ extended the break-through time to 10.5 h. At this temperature, the outlet concentration increased very slowly to 25% after 25 h. While the removal of SO_2 continued, some elusion of aq. H_2SO_4 was observed at outlet of the reactor. At room temperature of 30℃, SO_2 was completely removed at least 60 h while no SO_2 was observed at the outlet. Elusion of aq. H_2SO_4 was clearly observed at the outlet.

Figure 5 summarizes the influences of H_2O concentration on the break-through profiles of SO_2 through FE-300-800 at 100, 80 and 50℃. Higher concentration of H_2O (20 and 30 vol%) extended slightly the break-through time at 100℃ and allowed the stationary removal of SO_2 at the outlet after the concentration became steady. The stationary concentrations under 10 and 20 vol% H_2O were 100 and 80%, respectively. Higher concentrations of H_2O were more pronounced at 80 ℃. The stationary concentrations of SO_2 under 10, 20 and 30 vol% H_2O were 60, 55 and 10%, respectively while the break-through time was extended to 7 to 10 h. The influence of H_2O concentration was more drastic at 50℃. H_2O concentration of 20 vol% allowed a steady SO_2 removal of 100%, no SO_2 being detected for 60 h, whereas 10 vol% H_2O provided 30% steady concentration at the outlet. When the steady removal of SO_2 was achieved, elusion of aq. H_2SO_4 was observed. Hence, SO_2 is adsorbed, oxidized, and hydrated into aq. H_2SO_4 on the ACF surface which flows out from the bed to be stored in the reservoir at the reactor outlet (Fig.1). Thus, the removal of SO_2 is expected to continue. Enough water is necessary to hydrate SO_3 and to dilute H_2SO_4 to flow smoothly through the ACF bed.

Figure 6 summarized the influences of W/F (Flow rate was fixed at 100 ml min^{-1}) on the break-through profiles of SO_2 through FE-300-800 at 100 and 30℃ when humidity was fixed at 10 vol%. In the case of 100℃, break-through time (T_0) was extended drastically with increasing of W/F. When the weight of the ACF increased from 0.25 g to 1.0 g, T_0 was extended markedly from

1.8 h to 18 h. The concentration of SO_2 at the outlet was saturated to be 100% by 10-15 h when ACF of 0.25 and 0.5 g was used, respectively. When the ACF was increased to 1.0 g, SO_2 concentration at the outlet increased very slowly but continuously even 45 h after SO_2 adsorption started. Larger amount of ACF may allow the better contact of the gas with the fiber and some storage of adsorbed H_2SO_4 to fill the void in its bed.

The ACF removed SO_2 completely for 60 h at least by W/F = 5.0×10^{-3} g min ml^{-1} at 30℃. However, 0.25 g of ACF removed SO_2 completely for 2.0 h, and then SO_2 started to leak. SO_2 concentration in the outlet increased continuously to 10% by 7.5 h, and stayed at the level until 15 h at least, leaving aq. H_2SO_4 in the reservoir. The highest concentration of H_2SO_4 trapped in the reservoir at the outlet of the reactor, was 7.3 normal when the PAN-ACF-FE-300-800 was used at 30℃ with 10 vol% H_2O. The concentration should depend on the SO_2 concentration and conversion, and vol% of H_2O. Hence the ACF of the highest activity and the largest amount for the complete conversion and lower temperature which allows lower concentration of H_2O are favorable to increase the concentration of recovered H_2SO_4.

Discussion

The oxidation and hydration of adsorbed SO_2 were found to proceed on the ACF surface at a temperature range of 30-100℃. The surface of the activated carbon was found to oxidize SO_2 efficiently and rapidly. The key point of the present study is to achieve the continuous recovery of aq. H_2SO_4 by supplying H_2O vapor onto ACF. The results indicate that the necessary concentration of water vapor is very much dependent on the reaction temperature, being 20 vol% at 50℃ and 10 vol% at 30℃ when the W/F was large enough. Higher reaction temperature requires more supply of water. H_2SO_4 can flow only when it is diluted to a certain concentration by the sufficient water on the ACF surface. Water is condensed on the ACF from the gas phase basically according to the relative humidity, although H_2SO_4 itself may adsorb water.

Fiber form of ACF may be favorable for smooth flow of aq. H_2SO_4 through the adsorbent bed. Flue gas sometimes requires further reduction of NOx after the desulfurization. Hence the temperature of desulfurization should be balanced since higher temperature is favorable for the reduction while lower desulfurization temperature requires less water. The flow of aq. H_2SO_4 may depend also on the surface structure of ACF.

It is worthwhile to note that the heat-treatment at 800 ℃ increased significantly the ability of SO_2 recovery. The oxidation appears to be enhanced. Such treatment may introduce the active site for adsorption[6,7] and oxidation[10] of SO_2 through the evolution of CO and CO_2 by decomposition of surface oxygen functional groups on ACF. Another interesting point is that PAN-ACF showed much higher activity than pitch ACF. Their surface structure is interestingly compared. NO probably co-existing in the flue gas may pass through ACF bed with least oxidation under the present condition as discussed in the following paper. Hence we expect separate recoveries of H_2SO_4 and HNO_3.

References

1) Y. Miura, *Nenryo Kyokaishi*, 1978, **57**, 817.

2) K. Knoblauch, E. Richter, and H. Juntgen, *Fuel*, 1981, **60**, 832.

3) Y. Komatsubara, I. Shiraishi, M. Yano, and S. Ida, *Nenryo Kyokaishi*, 1985, **64**, 255.

4) I. Keiichiro, Y. Niwa, and Y. Morita, *Nenryo Kyokaishi*, 1985, **64**, 338.

5) I. Mochida, Y. Masumura, T. Hirayama, H. Fujitsu, S. Kawano, and K. Gotoh, *Nippon Kagaku Kaishi*, 1991, **1991**, 296.

6) I. Mochida, T. Hirayama, S. Kisamori, S. Kawano, and H. Fujitsu, *Langmuir*, 1992, **8**, 2290.

7) I. Mochida, S. Kisamori, S. Kawano, and H. Fujitsu, *Nippon Kagaku Kaishi*, 1992, **1992**, 1429.

8) S. Kisamori, S. Kawano, and I. Mochida, Extended Abstr., 21th Biennial Conf. on Carbon, 478, Buffalo, June 1993.

9) K. Yamamoto, K. Kaneko, and M. Seki, *Kogyo Kagaku Kaishi*, 1971, **74**, 84.

10)S. Kisamori, S. Kawano, and I. Mochida, *Langmuir*, in press.

11)S. Kisamori, S. Kawano, and I. Mochida, *Chemistry Letters*, 1993, **11**,1899.

Table 1. Some properties of ACFs

ACFs	Elemental Analysis(wt%)					Surface area
	C	H	N	O diff.	Ash	($m^2 g^{-1}$)
FE-100	77.5	1.8	9.7	11.0	0.3	446
FE-200	75.8	1.7	5.8	16.7	0.3	887
FE-300	78.1	1.4	4.5	16.0	0.3	1141
OG-5A	89.6	1.1	0.7	8.3	0.3	480
OG-10A	91.6	0.9	0.5	6.7	0.3	710
OG-20A	93.9	0.9	0.3	4.6	0.5	1150

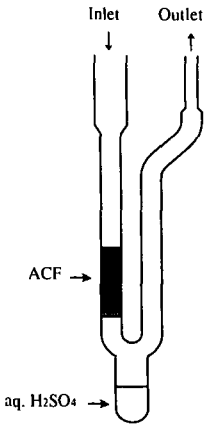

Fig.1 Reactor

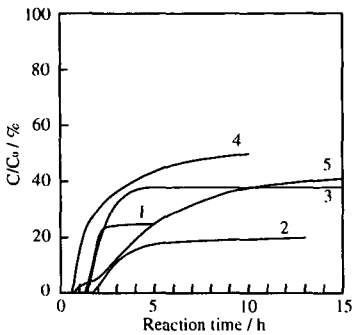

Fig.2 Breakthrough profiles of SO_2 over as-received ACFs
SO_2 1000ppm, O_2 5 vol%, H_2O 10 vol%
W/F = 5.0×10^{-3} g min ml^{-1}
Reaction temp. = 30℃
1 : FE-100 (PAN, 450$m^2 g^{-1}$)
2 : FE-300 (PAN, 1140$m^2 g^{-1}$)
3 : OG-5A (Pitch, 480$m^2 g^{-1}$)
4 : OG-10A (Pitch, 710$m^2 g^{-1}$)
5 : OG-20A (Pitch, 980$m^2 g^{-1}$)

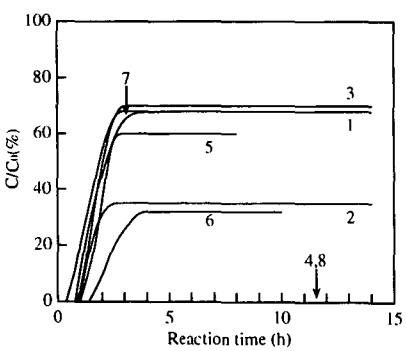

Fig.3 Breakthrough profiles of SO_2 over heat-treated FE-200 and FE-300 at 30℃
SO_2 1000ppm, O_2 5 vol%, H_2O 10 vol%
W/F = 2.5×10^{-3} g min ml^{-1} (1-3, 5-7)
5.0×10^{-3} g min ml^{-1} (4, 8)
1 : FE-200-600; 2,4 : FE-200-800; 3 : FE-200-1000
5 : FE-300-600; 6,8 : FE-300-800; 7 : FE-300-1000

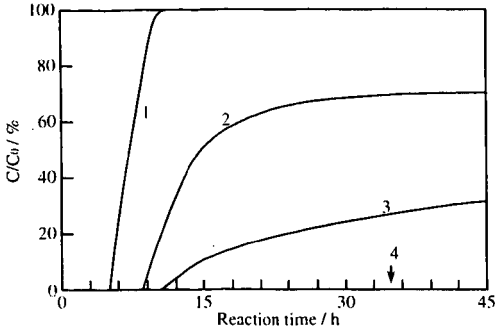

Fig.4 Breakthrough profiles of SO_2 at several temperatures over FE-300-800
SO_2 1000ppm, O_2 5 vol%, H_2O 10 vol%
W/F = 5.0×10^{-3}g min ml^{-1}
1 : 100℃, 2 : 80℃, 3 : 50℃, 4 : 30℃
No.4 adsorbed SO_2 completely for least 60 hours

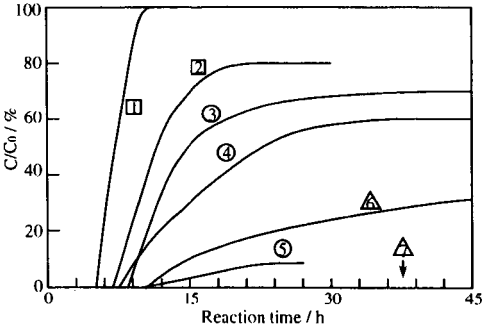

Fig.5 Effect of H_2O concentration for SO_2 removal over FE-300-800
SO_2 1000ppm, O_2 5 vol%, W/F = 5.0×10^{-3}g min ml^{-1}
1 : 100℃, H_2O 10 vol%, 2 : 100℃, H_2O 20 vol%,
3 : 80℃, H_2O 10 vol%, 4 : 80℃, H_2O 20 vol%,
5 : 80℃, H_2O 30 vol%, 6 : 50℃, H_2O 10 vol%,
7 : 50℃, H_2O 20 vol%
No.7 adsorbed SO_2 completely for least 60 hours

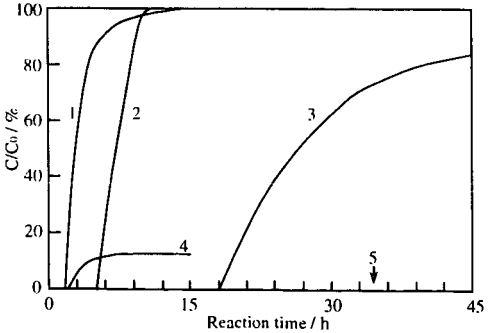

Fig.6 Influence of W/F for SO_2 removal of FE-300-800
SO_2 1000ppm, O_2 5 vol%, H_2O 10 vol%
1 : 100℃, W/F=2.5×10^{-3}g min ml^{-1}
2 : 100℃, W/F=5.0×10^{-3}g min ml^{-1}
3 : 100℃, W/F=1.0×10^{-2}g min ml^{-1}
4 : 30℃, W/F=2.5×10^{-3}g min ml^{-1}
5 : 30℃, W/F=5.0×10^{-3}g min ml^{-1}

CATALYTIC REDUCTION OF SULFUR DIOXIDE TO ELEMENTAL SULFUR

Yun Jin, Qiquan Yu, and S. G. Chang, Energy and Environment Division, Lawrence Berkeley Laboratory, University of California Berkeley, CA 94720

Keywords: sulfur dioxide, catalytic conversion, elemental sulfur

INTRODUCTION

There are several regenerable flue gas desulfurization processes; some of them have been commercilized, while others are still emerging. In the regenerable processes, sulfur dioxide from flue gas is first absorbed into an alkaline solution (Wellman-Lord, Tung, Cansolv, and Dow processes) or adsorbed on a solid substrate (NOXSO and CuO processes), and is subsequently desorbed to produce a stream of high concentration sulfur dioxide. It is desirable to convert sulfur dioxide to elemental sulfur for storage, transportation, and/or conversion to valuable chemicals.

Sulfur dioxide can be reduced with synthesis gas, derived from coal ($H_2/CO = 0.3\text{-}1.0$) or methane ($H_2/CO = 3$), to produce elemental sulfur at elevated temperatures according to the reaction

$$0.875\ SO_2 + 0.75\ H_2 + CO \text{ ----------> } 0.438\ S_2 + CO_2 + 0.75\ H_2O \quad (1)$$

$$2\ SO_2 + 3\ H_2 + CO \text{ ----------> } S_2 + CO_2 + 3\ H_2O \quad (2)$$

These reactions are facilitated with catalysts. In addition to elemental sulfur, these reactions may produce several undesirable byproducts. These include hydrogen sulfide, carbonyl sulfide, carbon disulfide, and elemental carbon. Numerous research efforts have been carried out to develop catalysts for these reactions so that they can proceed with high conversion of sulfur dioxide and high selectivity to elemental sulfur at low temperatures. However, the results obtained so far show only limited successes and do not warrant a commercial application. Using synthesis gas to reduce SO_2, Akhmedov et. al. [1] developed several catalysts and obtained the following results: a 64-65 % sulfur yield with a bauxite-bentonite catalyst at 350 C with a feed gas at a molar ratio ($CO + H_2$)/SO_2 of 2 and a space velocity of 1000 h^{-1}; a 82.0 % sulfur yield with a NiO/Al_2O_3 catalyst at 300 C with a space velocity of 500 h^{-1} [2]; a 82.0 % and 87.4 % sulfur yield with a Co_2O_3/Al_2O_3 catalyst [3] at 300 C with a space velocity of 1000 h^{-1} and 500 h^{-1} respectively; a 82.3 % and 78.6 % sulfur yield with a $NiO+Co_3O_4$ catalyst [4] at 400 C with a space velocity of 500 h^{-1} and 1000 h^{-1} respectively. The development of a catalyst capable of obtaining better than 90 % yield of sulfur with a high space velocity at low temperatures would be required to warrant a commercial application. This paper reports the evaluation results of a promising catalyst formulated in our lab.

EXPERIMENTAL

Catalyst Preparation

Catalysts were composed of a combination of several metal oxides supported on $-Al_2O_3$. Two sizes of $-Al_2O_3$ were used: 1. 30-40 mesh particles, and 2. 3mm dia. by 5 mm height granules. By mixing appropriate amounts of metal nitrate solutions with $-Al_2O_3$, the mixture underwent stepwise heating to form the activated catalyst. The ratio of the active catalyst to carrier was about 0.3 by weight.

Apparatus and Procedure

A schematic flow diagram of the apparatus is shown in Figure 1. The experimental setup consists of three separate sections: the gas supply section, the main reactor, and the detection and analysis section. Gases are supplied from compressed gas cylinders (Matheson Gas Products) to gas flow meters before entering a gas mixer. The tubular reactor is fabricated from a 1.4-cm-o.d. with a 1-mm wall thickness quartz tube. The entire reactor is mounted inside a tubular furnace. The reactor, which is 5 cm long, consists of three zones. The inlet or the preheating zone (2.5 cm long) is packed with 20 mesh quartz chips, the reaction zone (1.5 cm long) is packed with either particles (30-40 mesh) or granules (d. 3mm x h. 5mm) activated catalysts on alumina, and the outlet zone (1 cm long) is packed with quartz chips (20 mesh), mainly for the purpose of supporting the catalyst, which sat on a perforated quartz plate having seven holes for gas exit. A thermocouple, reaching the center of the catalytic packing, provide measurement of the temperature of catalytic reactions. After the last section of the reactor, the gases pass through a sulfur collector at room temperatures, and then enter into an on-line trap cooled in an ice bath to condense water before entering a six-port sampling valve which is used to inject the products of the catalytic reactions into the gas chromatograph. Finally, the exit gases pass into a scrubber containing concentrated NaOH.

The inlet and exit gases are analyzed by using a gas chromatograph equipped with a column switching valve and a thermal conductivity detector. A 2-meter Porapak QS (80-100 mesh) column was employed. The operating conditions were at 60 mA and at column temperature of 100 C. The carrier gas is helium.

RESULTS AND DISCUSSION

The inventive catalyst (Cat-S) consists of active metal oxide components and carriers (-Al_2O_3). In order to study the kinetics of the reactions and the diffusivity of the reactants, two carrier sizes were used. The smaller size carrier is 30-40 mesh -Al_2O_3 particles, which were used typically in laboratory scale experiments to obtain kinetic information. The larger size carrier has a dimension of 3 mm diameter by 5 mm height cylindrical granules, which were used in scale up tests. The parametric studies were conducted on particles and granules for comparison. The lifetime experiments were performed on particles.

Particles (30-40 mesh)

Parametric Studies

The effect of temperatures, space velocity, molar ratios of reductants to SO_2 ($R = F_{(H2+CO)}/F_{SO2}$), and molar ratios of H_2 to CO ($r = F_{H2}/F_{CO}$) on the activity of the catalyst (Cat-S) were investigated in order to determine the optimum operating conditions.

Tables 1 and 2 summarize the results of temperature dependence studies at a space velocity of 10,000 h^{-1} and 15,000 h^{-1}, respectively. The experiments were carried out at r = 3, and R = 2. The results show that the conversion of SO_2 is > 95 % when the temperature is > 380 C at both space velocities. Over the temperature range (340 C - 480 C) studied, the yield of H_2S does not show any appreciable and systematic changes: between 0.716 % and 3.31 % at a S.V.=10,000 h^{-1}, and between 0.919 % and 4.96 % at a S.V.=15,000 h^{-1}. However, the yield of COS shows a decrease with an increase of temperatures: Y_{COS} =2.75 % and 0.749 % at 340 C and 480 C, respectively (at a S.V.=10,000 h^{-1}); Y_{COS} =10.5 % and 0.178 % at 340 C and 480 C, respectively (at a S.V.=15,000 h^{-1}). AT a S.V.=10,000 h^{-1}, the yield of elemental sulfur, Y_{S2} is 93.7 % at 380 C and reaches a maximum value of 95.1 % at 420 C; it decreases slightly to 94.4 % with further increase of the temperature to 480 C. At a S.V.=15,000 h^{-1}, Y_{S2} is 92.8 % at 380 C, and reaches 94.9 % at 420 C.

The effect of space velocity on the catalyst was shown in Table 3. The conversion of SO_2 remains fairly stable (95.8 % - 98.7 %) in a S.V. range of 5,000 to 15,000 h^{-1}. At a S.V. =15,000 h^{-1}, it was observed that the temperature of the catalyst increased 60 degree C, which could be attributed to the liberation of heat from the reactions (exothermic reactions). Y_{H2S} remains at very low level (0.269 % - 0.716 %) when the S.V. is less than 10,000 h^{-1}, it shows a slight increase to 2.21 % as the S.V is increased to 13,750 h^{-1}, but it reaches 4.96 % as the S.V. is further increased to 15,000 h^{-1}. Y_{COS} remains very small (0.095 % - 1.32 %), and does not appeared to be affected systematically by the change of the space velocity. Y_{S2} remains very high value (95.1 % -97.5 %) for S.V. up to 13,750 h^{-1}, it decreases to 92.3 % when the S.V. is increased to 15,000 h^{-1}.

Lifetime tests

The lifetime test was carried out continuously for 1080 h (45 days). The flow rate of H_2, CO, and SO_2 were 2286, 3047, and 2667 ml/h respectively. These correspond to R=2 and r=0.75. The amount of catalyst used was 1 g. These correspond to a space velocity of 10,000 h^{-1}. The catalytic activity was evaluated at three temperatures: 440, 460, and 480 C. The arithematic mean of the experimental results of all 45 days is shown in Table 4. Also given in Table 10 is the arithematic mean of results of an additional experimental condition which was implemented after 15 days lifetime test , and used r =3 to cover the composition of synthesis gas produced from methane.

The results indicate that the activity of the Cat-S, including the conversion and the selectivity, is very stable and does not show any changes during the entire 1080 h of the lifetime test. Table 10 shows that the yield of elemental sulfur ranges between 93.1 and 96.5 %, which is far superior to results so far reported in the literatures [2,3,4]. These high yields were achieved at a space velocity of 10,000 h^{-1} , compared with a reported result of obtaining 69.3 - 72.8 % yield of elemental sulfur at a space velocity of 2,000 h^{-1}, and a 82.8 % sulfur yield at a space velocity of only 500 h^{-1}. Table 10 shows that the yield of H_2S ranges between 1.28 and 2.82 %, which is far better than those of other catalysts: 13.4 % for NiO/Al_2O_3 [2] at a space velocity of 2000 h^{-1} and at 400 C; 3.80 % for Co_2O_3/Al_2O_3 [3] at a space velocity of 2000 h^{-1} and at 300 C; 13.9 % for NiO + Co_3O_4 [4] at a space velocity of 2000 h^{-1} and at 450 C. The yield of H_2S increases along with the increase of the reaction temperatures. Therefore, it is remarkable to observe the low yield of H_2S for the Cat-S at a temperature of 440 to 480 C.

Granules (d. 3 mm x h. 5 mm)
Parametric Studies
The effect of temperature, space velocity, and molar ratio of reactants on the activity and selectivity of the Cat-S catalyst on granules was studied. Table 5 and 6 show the effect of temperature on the catalyst at r = 0.4 and 3 respectively. The results indicate that at a given temperature, C, Y_{S2}, and S_{S2} increase, while Y_{H2S} and Y_{COS} decrease along with the increase of r. Meanwhile, C, Y_{H2S}, and S_{S2} show an increase, while Y_{COS} decreases, as the reaction temperature is increased at a given r value. At a space velocity of 2100 h^{-1} and R = 2 (i.e. a stoichiometric ratio), the yield of sulfur increases to more than 90% when the temperature is above 560 C, 520 C, and 460 C with r = 0.4, 0.75, and 3 respectively. It is worthy noting that the yield of sulfur reaches 97.8% at 560 C and a space velocity of 2100 h^{-1} with synthesis gas derived from methane (i.e. r = 3).

The effect of the space velocity on the catalyst for r = 3 was shown in Table 7 (480 C). The temperature of this series of experiments were chosen such that Y_{S2} could achieve more than 90%. The results indicate that C, Y_{H2S}, and Y_{S2} decrease, while Y_{COS} increases along with the increase of the space velocity. S_{S2} remains fairly constant under the experimental conditions employed.

The effect of R on the Cat-S at r = 3 was summarized in Table 8 (480 C). The results show that at a given r value, C, Y_{H2S}, and Y_{COS} show a slight increase along with the increase of R until R reaches 2. Beyond that however, Y_{H2S} exhibits a drastic growth with the increase of R; Y_{COS} also shows some growth with R, but to a much lesser extent than Y_{H2S}. It is obvious that Y_{S2} is the greatest when R is 2 regardless of the ratio of r.

High Efficiency Recovery
Because of the incomplete conversion of SO_2, and the production of unwanted byproducts, H_2S and COS, either a tail gas treatment step or recycling the byproducts for combustion is necessary. Many technologies have been developed for the treatment of tail gas from a Claus process. However, the tail gas treatment cost is substantial. The combustion treatment would increase the concentration of SO_2 in flue gas. Therefore, it is desirable to maximize the yield of elemental sulfur and to minimize the production of byproducts.

The operating conditions of the Cat-S to obtain a Y_{S2} of 97 % have been determined. Table 9 and 10 show the effect of space velocity and temperature on the catalytic reduction of SO_2 by synthesis gas derived from methane to achieve a more than 93% Y_{S2}. Y_{S2} reaches between 96.9% and 97.1% at 520 C and a space velocity from 1,800 h^{-1} to 2,000 h^{-1}; further increase of space velocity to 3,000 h^{-1}, Y_{S2} decreases to 93%. To achieve a Y_{S2} of 96% at a space velocity of 3,000 h^{-1}, the temperature of the catalytic reactions would have to be increased to 580 C (Table 28).

An alternative technology for the conversion of SO_2 to elemental sulfur involves two steps: 1. the combustion of SO_2 in a hydrocarbon flame under reduced conditions to form H_2S, 2. the employment of a Claus process to react SO_2 with H_2S to produce elemental sulfur. The first step requires the consumption of an excess amount of hydrocarbon, compared with the need of only a stoichiometric amount of synthesis gas for SO_2 reduction in the present invention. The Claus process requires three stages to achieve a 96-97% Y_{S2} at a space velocity of 1,500 -3,000 h^{-1}, while the new technology needs only a single stage reactor to obtain the same Y_{S2} at a comparable space velocity, 2,000 - 3,000 h^{-1}.

CONCLUSION
We have developed a catalyst for reduction of SO_2 by synthesis gas. This catalyst is composed of a mixture of common transition metal oxides supported on -alumina and is inexpensive.

The inventive catalyst can achieve a high conversion efficiency of SO_2 by synthesis gas with a high selectivity to elemental sulfur. Unlike the Claus process, the reaction of SO_2 with synthesis gas to form elemental sulfur is not a reversible process. As a result, a high efficiency recovery of sulfur can be achieved in a single stage reactor.

A lifetime (1080 h) test has been successfully performed on the Cat-S in 30-40 mesh particle sizes. The test was conducted at 480 C, S.V. = 10,000 h^{-1}, R = 2, and at r = 3 and 0.75. The activity of the catalyst remains very stable during the entire period of the lifetime test. The yield of sulfur was 96.5% and 94.1% at r = 3 and 0.75 respectively.

The mass balance of sulfur and carbon has been checked satisfactory by measuring the aforementioned products.

It has been demonstrated that the byproducts, H_2S and COS, produced during the conversion of SO_2 to sulfur can be circulated back to the feed gas for subsequent conversion on inventive catalysts without resulting in further accumulation of the said byproducts.

This catalyst can achieve 97% yield of elemental sulfur at 540 C with a space velocity of 2,000 h^{-1} or at 640 C with a space velocity of 3,000 h^{-1}. This catalyst requires only a stoichiometric amount of synthesis gas for SO_2 reduction. While the waste of fuel is negligible, the operating cost is small

The inventive catalyst possesses very promising properties. As such, it could be utilized as a basis to develop a new process for high efficiency conversion of SO_2 to elemental sulfur by synthesis gas at a more cost effective manner than technologies available currently.

REFERENCES

(1). Akhmedov, M.M., Shakhtakhtinskii, G. B., Agaev., A.I., Azerb. Khim. Zh. (2) 95 (1983).
(2). Akhmedov, M.M., Gezalov, S.S., Agaev, A.I., Mamedov, R.F., Zh. Prikl. Khim., 61, (1) 16 (1988).
(3). Akhmedov, M.M., Guliev, A.I., Agaev, A.I., Gezalov, S.S., Zh. Prikl. Khim., 61, (8) 1891 (1988).
(4). Akhmedov, M.M., Guliev, A.I., Ibragimov, A.A., Khim. Prom. (1), 37 (1989).

ACKNOWLEDGEMENT

The authors appreciate the support of Perry Bergman, Charles Schmidt, and Charles Drummond. This work was supported by the Assistant Secretary for Fossil Energy, U.S. Department of Energy, under Contract DE-AC03-76SF00098 through the Pittsburgh Energy Technology Center, Pittsburgh, PA.

Table 1 The effect of temperatures on the Cat-S(particles) at (H2/CO)=3.0, and S.V.=10,000 h^{-1}

t (°C)	C (%)	Y_{H2S} (%)	Y_{cos} (%)	Y_{S2} (%)	S_{S2} (%)
340	83.7	1.59	2.75	79.4	94.8
380	95.9	1.66	0.548	93.7	97.7
400	97.9	3.31	0.325	94.2	96.3
420	98.0	2.51	0.314	95.1	97.0
440	97.2	2.19	0.341	94.7	97.4
460	96.3	1.57	0.326	94.4	98.0
480	95.8	0.716	0.749	94.4	98.5

Table 2 The effect of the temperatures on the Cat-S (particles) at (H2/CO)=3.0, and S.V.=15,000 h^{-1}

t (°C)	C (%)	Y_{H2S} (%)	Y_{cos} (%)	Y_{S2} (%)	S_{S2} (%)
340	62.7	0.919	10.5	51.4	81.8
360	74.2	0.218	5.23	68.8	92.7
380	94.8	1.53	0.526	92.8	97.8
400	96.5	1.62	0.489	94.4	97.8
420	97.7	2.45	0.324	94.9	97.2
440	96.9	2.07	0.351	94.5	97.5
460	96.3	1.83	0.363	94.1	97.7
480	97.4	4.96	0.178	92.3	94.7

Table 3 The effect of the space velocity on the Cat-S (particles) at (H2/CO)=3.0, and 480 C

S.V. (h^{-1})	C (%)	Y_{H2S} (%)	Y_{cos} (%)	Y_{S2} (%)	S_{S2} (%)
5000	97.7	0.289	0.095	97.4	99.0
6250	98.2	0.482	0.123	97.5	99.4
7500	97.9	0.349	0.839	96.7	98.8
8750	98.4	0.574	0.102	97.7	99.3
10000	95.8	0.716	0.746	94.4	98.5
11250	96.6	0.269	0.077	96.2	99.6
12500	98.7	2.29	1.32	95.1	96.3
13750	98.5	2.21	0.248	96.0	97.5
15000	97.4	4.96	0.178	92.3	94.7

Table 4 The arithmatic mean values of the lifetime test results at 440 C, 460 C, and 480 C; and at the feed gas molar ratio (H2/CO)=0.75 [* feed gas molar ratio (H2/CO)=3]

t (°C)	C (%)	Y_{H2S} (%)	Y_{cos} (%)	Y_{S2} (%)	S_{S2} (%)
440	95.7	2.30	0.356	93.1	97.0
460	96.2	2.36	0.376	93.5	97.2
480	97.3	2.82	0.366	94.1	96.7
480*	98.2*	1.28*	0.382*	96.5*	98.3*

Table 5 The effect of the temperatures on the Cat-S (granules) at (H2/CO)=0.4, [(H2+CO)/SO2]=2.0, and S.V.=2,105 h^{-1}

t (°C)	C (%)	Y_{H2S} (%)	Y_{cos} (%)	Y_{S2} (%)	S_{S2} (%)
440	81.4	0.949	9.0	71.9	87.1
460	85.7	0.992	6.09	78.6	91.7
480	88.2	1.08	4.95	82.1	93.1
500	91.7	1.37	3.56	86.8	94.6
520	93.0	1.40	2.93	88.7	95.3
540	93.5	1.42	2.42	89.7	95.9
560	94.3	1.53	2.22	90.5	96.1
580	96.7	2.47	2.17	92.0	95.3

Table 6 The effect of the temperatures on the Cat-S (granules) at (H2/CO)=3.0, [(H2+CO)/SO2]=2.0, and S.V.=2,105 h^{-1}

t (°C)	C (%)	Y_{H2S} (%)	Y_{cos} (%)	Y_{S2} (%)	S_{S2} (%)
440	91.4	0.414	2.80	88.2	96.5
460	93.0	0.423	2.29	90.3	97.1
480	94.4	0.442	1.88	92.1	97.5
500	97.0	0.438	1.37	95.5	98.1
520	97.7	0.516	1.13	96.1	98.3
540	98.5	0.524	1.00	96.9	98.3
560	99.3	0.740	0.782	97.8	98.4
580	99.4	0.811	0.748	97.8	98.4

Table 7 The effect of the space velocity on the Cat-S (granules) at (H2/CO)=3.0, [(H2+CO)]/SO2]=2.0, and 480 C

S.V. (h^{-1})	C (%)	Y_{H2S} (%)	Y_{cos} (%)	Y_{S2} (%)	S_{S2} (%)
1000	98.6	2.35	0.789	95.5	96.8
1500	97.3	0.791	1.05	95.5	98.1
1800	96.0	0.696	1.52	93.8	97.7
2000	94.4	0.442	1.88	92.1	97.5
2500	90.6	0.619	1.96	88.0	97.2
3000	86.5	0.623	2.26	83.7	96.7

Table 8 The effect of the molar ratio of reactants on the Cat-S (granules) at (H2/CO)=3.0, [(H2+CO)]/SO2]=2.0, S.V.=2,000 h^{-1}, and 480 C

$\frac{CO + H_2}{SO_2}$	C (%)	Y_{H2S} (%)	Y_{cos} (%)	Y_{S2} (%)	S_{S2} (%)
3.0	99.8	35.1	1.59	63.2	63.3
2.5	99.7	21.0	1.64	77.0	77.3
2.2	99.8	6.61	1.72	91.4	91.7
2.0	94.4	0.442	1.88	92.1	97.5
1.8	92.9	0.339	1.64	91.0	97.9
1.6	88.9	0.293	1.66	87.6	97.8
1.4	84.1	0.302	1.63	82.8	97.7

Table 9 The effect of the space velocity on the Cat-S (granules) at (H2/CO)=3.0, [(H2+CO)]/SO2]=2.0, and 520 C

S.V. (h^{-1})	C (%)	Y_{H2S} (%)	Y_{cos} (%)	Y_{S2} (%)	S_{S2} (%)
1000	98.5	0.990	0.467	97.0	98.5
1500	98.2	0.445	0.772	96.9	98.8
1800	98.9	1.05	0.791	97.1	98.1
2000	98.5	0.624	1.00	96.9	98.3
2500	97.3	0.342	1.24	95.7	98.4
3000	94.8	0.337	1.47	93.0	98.1

Table 10 The effect of the temperatures on the Cat-S (granules) at (H2/CO)=3.0, [(H2+CO)/SO2]=2.0, and S.V.=3,158 h^{-1}

t (°C)	C (%)	Y_{H2S} (%)	Y_{cos} (%)	Y_{S2} (%)	S_{S2} (%)
540	95.3	0.479	1.30	93.5	98.1
560	96.1	0.536	1.06	94.5	98.3
580	97.6	0.614	1.00	96.0	98.3
600	98.3	0.979	0.882	96.5	98.1
620	98.4	0.920	0.755	96.8	98.3
640	98.6	0.931	0.621	97.0	98.4
660	98.8	1.36	0.441	97.0	98.2

THE EFFECT OF NONUNIFORM LIQUID DROPLETS CONCENTRATION DISTRIBUTION ON ABSORPTION OF SO2 IN AN ATOMIZING SCRUBBER

M.Taheri, J.Fathikalajahi,and M.R. Talaie

Shiraz University, Shiraz,Iran

Keywords: Drop Distribution, Scrubber, Absorption

ABSTRACT

Many investigators have predicted SO2 absorption in a scrubber based on uniform concentration of liquid droplets concentration. In this study an investigation was carried out to determine the effect of actual liquid droplets concentration on SO2 absorption in an atomizing scrubber. In this model liquid droplets are dispersed in the polluted gas stream from an area or line source depending on the method of liquid injection. Then the overall performance of the scrubber is obtained by solving the diffusion equation both for liquid droplets and gas absorption. The effect of various operating parameters such as liquid to gas ratio and scrubber size were obtained on cleaning performance of the scrubber. The results of mathematical predictions is compared with the data reported in the literature. The results of prediction with this model indicate a significant improvement compare to the prediction based on uniform liquid droplets concentration.

INTRODUCTION

Atomizing scrubbers are frequently used for absorption of SO2 and some other gaseous pollutants. Gage and Rochelle (1992) have studied the use of this device in flue gas desulphurization processes.Also the capital cost and operating cost of a scrubber is given by Baasel (1988). In an atomizing scrubber the performance of gas absorption is a function of several parameters including ,gas velocity, liquid to gas flow rate ratio, geometry, and the method of liquid injection. In designing a venturi scrubber the above parameters must be adjusted so that the liquid droplets are distributed as uniformly as possible. The purpose of this study was to study the effect of various operating parameters on liquid droplets concentration distribution in a scrubber. This in turn will improve the capability of various mathematical models in predicting gas absorption and particulate removal in a wet scrubber.

Several experimental and theoretical investigations for studying droplets concentration distribution in atomizing scrubbers have been reported in the literature. Taheri and Haines carried out an experimental work to study the effect of water injection on droplets distribution and SO2 absorption in an atomizing scrubber. By photographing the throat of scrubber they showed that the water droplets are distributed nonuniformly across the cross section of scrubber. They also showed that the rate of SO2 absorption and particle collection varied depending on method of water injection. Viswanathan et.al (1984) performed experimental work for determining water droplets distribution in the throat of a venturi scrubber. They showed that the droplets concentration distribution in the throat and down stream of point of water injection is a function of liquid to gas ratio. Calvert(1970) developed a mathematical model to predict particulate removal efficiency in a scrubber. He fitted the results of the experimental work by applying a correction factor in his model which included the non-uniformity effect of droplets distribution. Taheri and Shieh (1975) used a plume dispersion equation to predict water droplets concentration in an atomizing scrubber. They have shown that by considering nonuniform distribution of droplets the particulate removal efficiency are in close agreement with experimental data.

MATHEMATICAL MODEL

The detail of the mathematical model developed in this work is

given by Talaei (1993). This model is based on a three dimensional dispersion of droplets and pollutants such as SO2 by convection and eddy diffusion. The gaseous pollutants are absorbed by liquid droplets while they are moving co-currently in the scrubber. The rate of gas absorption in the scrubber is influenced by distribution of droplets population. The steady state equation expressing material balance for droplets is as follows:

$$\frac{\partial(V_{d_x})}{\partial x} = E_d\left(\frac{\partial^2 C_d}{\partial y^2} + \frac{\partial^2 C_d}{\partial z^2}\right) + S \qquad (1)$$

In the above equation the droplets are convected in the x direction, while they are dispersed in y and z direction by eddy diffusion. In addition it is assumed that droplets are generated by a line or area source depending on method of water injection. This area source is located by an empirical correlation for calculating liquid jet penetration length which has been obtained by Viswanathan et.al (1984):

$$\frac{h^*}{d_j} = 0.1145\frac{V_j\rho_j}{V_g\rho_g} \times \left(\frac{P_j}{P_g}\right)^{1/2} \qquad (2)$$

The water droplets velocity V is adjusted to the ambient gas stream velocity according to the following equation:

$$\frac{dV_d}{dX} = \frac{3}{4}\frac{C_{D_\ell}}{D_d}\frac{\rho_g}{\rho_l}\frac{(V_g - V_d)^2}{V_d} \qquad (3)$$

The Transport equation for gaseous pollutant such as SO2 is as follows:

$$\frac{\partial(V_{g_x}C_g)}{\partial x} = E_g\left(\frac{\partial^2 C_g}{\partial y^2} + \frac{\partial^2 C_g}{\partial z^2}\right) - N_A\pi D_d^2 C_d \qquad (4)$$

The eddy diffusivity E depends on the flow situation and is a function of the degree of mixing and turbulence. The gas stream eddy diffusion was obtained by using a Peclet number :

$$\frac{V_g D}{E_g} = N_{Pe} \qquad (5)$$

The value of Pecklet number was found to be 130 for a venturi scrubber. Droplets because of their inertia can not follow the random motion of gas stream. As a result their eddy diffusion is reduced. The effect of droplets inertia on eddy diffusivity was obtained by Talaie (1993):

$$\frac{E_d}{E_g} = \frac{l_d^2}{l_g^2} \qquad (6)$$

NUMERICAL SOLUTION

Equations (1),(2) and (3) are the main equations for the present model.Equation (3) is integrated analytically and the droplets velocity U is computed. With all the other parameters Known , the problem is then reduced to solving C,and C by a numerical technique.

RESULTS

The comparison between the result of simulation and Viswanathan

data for water droplets distribution is given in Figure (1). This Figure indicates a very good agreement between predicted value s and experimental data.
Figure (2) indicates the comparison between Calculated and experimental data performed by The Office of Air Program. These data are reported by Wen and Fan (1975). This figure indicates a very good agreement compare to applying a uniform water droplets concentration. The results indicate that water droplets concentration distribution plays an important role in scrubber performance and must be considered in any realistic model.

SUMMERY AND CONCLUSION

From the results of simulation the following conclusions can be drawn:
The factors which increases the uniformity of droplets distribution also increases removal efficiency.The highest uniformity of droplets distribution is attained in a scrubber for a jet penetration of 20 to 30% of scrubber width. Some of the factors which affects the uniformity of droplets distribution are as follows:
a) Increasing liquid to gas flow ratio, to some limit at constant gas velocity increases uniformity
b) When L/G and Vg are constant,increasing cross sectional area of the scrubber increases uniformity by increasing droplets eddy diffusivity.

ACKNOWLEDGEMENT

This research was supported by Shiraz University Research Council.

NOTATION

C	=	Droplets concentration	No./m^3
C	=	Gas concentration	gmole/m^3
D	=	Throat diameter of scrubber	m
D	=	Drop diameter	m
d	=	Nozzle diameter	m
E	=	Eddy Diffusivity	m^2/s
h	=	Penetration length	m
l	=	Mixing length	m
L/G	=	Liquid to gas flow rate ratio	m^3/1000 m^3
N	=	Overall mass transfer rate of component A	gmole/m^2.s
P	=	Pressure of liquid jet at injection point	(atm)
S	=	Source strength	No./m^2.s
V	=	Velocity	m/s
x	=	Rectangular coordinate in the direction of flow	m
y,z		Rectangular coordinate perpendicular to the direction of flow	m

Subscripts

d	=	Droplets
g	=	Gas
J	=	Jet

References

Baasel,W.D. (1988) Journal of Air Pollution Control Association, Volume 38,327
Calvert,S.(1970) AIChE Journal,16,392
Gage,C.L., and G.T. Rochelle,(1992) Journal of Air and Waste Management Association, Volume 42,926
Taheri,M. and G.F. Haines,(1969) Journal of Air Pollution Control Association,19,427
Taheri,M., and C.M.S. Sheih,(1975),AIChE Journal,21,153

Talaei,M.R.(1993) M.S. Thesis, Chemical Engineering Department, Shiraz University, Shiraz,Iran
Viswanathan,S,A.W.Gnyp, and C.C.St. Pierre.(1984) Ind.Eng.Chem. Fundamental,23,303
Wen, C.Y.,and L.T. Fan, (1975)"Models for flow systems and chemical reactors",Marcel Dekker Inc.New York

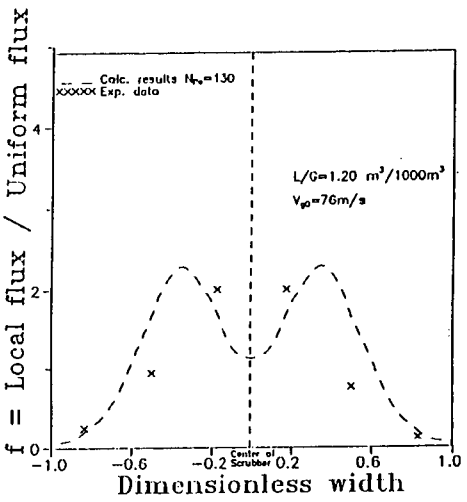

Figure 1 Variation of Normalized Flux With Dimensionless Width

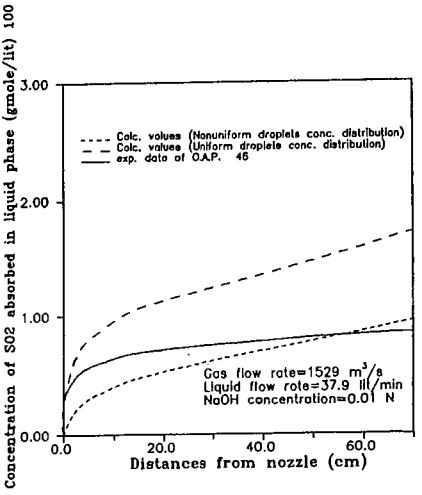

Figure 2. Variation of Liquid Phase Concentration Along the Scrubber for O.A.P. Data

PhOSNOX PROCESS FOR COMBINED REMOVAL OF SULFUR DIOXIDE AND NITROGEN OXIDES FROM FLUE GAS

S.G. Chang and S. M. Wang , Energy and Environment Division, Lawrence Berkeley Laboratory, University of California, CA 94720, U. S. A.

Keywords: nitric oxide, flue gas cleanup, phosphorus

INTRODUCTION

Wet FGD (flue gas desulfurization) systems are the most widely used technology for control of sulfur dioxide emissions from power plants. However, these systems are incapable of removing nitrogen oxides because most of the nitrogen oxides in flue gas is nitric oxide which is barely soluble in aqueous solutions.

This paper addresses a new and cost-effective method for the generation of ozone to allow a wet scrubber system to remove SO_2 and NO_x simultaneously. In addition, a new method to suppress the formation of nitrogen-sulfur compounds in scrubbing liquors is discussed. The major oxidation product of yellow phosphorus is phosphoric acid mists which can be recovered for byproducts credit. The size of mists and the concentration of phosphoric acid in the mists were measured in order to determine an appropriate device for acid collection and concentration. An economic projection of the PhoSNOX process has been performed.

EXPERIMENTAL

The experiments were conducted on a 600 liter/min bench-scale spray tower absorber. A simulated flue gas mixture with about 5% oxygen was prepared by passing liquid nitrogen through a vaporizer column and by mixing the gas with compressed air to obtain the desired oxygen concentration. NO and SO_2 were blended in to give concentration of 60-600 ppm and 1500-2500 ppm, respectively. CO_2 concentration could be adjusted up to approximately 10% of the total gas flow. The gas stream flowed at a rate of 600 liter/min through an electric air heater where it was heated to a temperature of 450 K (350 F). The heated gas then entered a spray tower absorber. The absorber was a 10 cm diameter by 120 cm long glass column installed with spray nozzles (Figure 1). A scrubbing liquor, which was composed of an aqueous mixture of yellow phosphorus was sprayed in the absorber. The liquid flow rate ranged between 1 and 4 gallons/min. A 2-liter Erlenmeyer flask was used as a holding tank for the liquid mixture from the spray column. The liquid mixture was recirculated with a centrifugal pump to the top of the spray column. The pH of the scrubbing liquor was controlled by feeding an aqueous mixture of sodium sulfite or calcium carbonate from a thermostated reservoir (55 C) to the hold tank by a Masterflex pump. The pH range studied was 4.5 to 7.5. The holding tank temperature was controlled at 55 C. A countercurrent flow of flue gas entered at the base of the absorber and passed upward through the falling spray of liquors. The superficial velocity of flue gas in the absorber is about 4 ft/sec. The contact time of flue gas with spraying solution was approximately 2 seconds. The contact time can be varied by changing the flow rate of flue gas; correspondingly, this would vary the L/G ratio, given a constant liquid flow rate. The SO_2 fluorescent analyzer and the NO_x chemiluminescent analyzer have intake connections to the gas stream at various points along the system. The SO_2, NO, and NO_2 concentrations can thus be measured and the effectiveness of the absorber operation can be evaluated.

The major oxidation product of P_4 is phosphoric acid mists which can be recovered as a valuable commercial product. Experiments were performed to determine the size distribution of mists in order to determine an appropriate collector for use in scale-up tests. The size of mists was measured by means of a cascade impactor and a laser optical particle counter. The mists produced from the bench-scale spray tower flowed through thermostated tubings. Then, the mists were sucked into a Mark V Pilat Cascade Impactor, which was installed inside an oven at a controlled temperature. The application of the laser optical particle counter has limitations in that it can not measure particles with size less than 0.5 um, nor can it measure particles with density more than 10^6 particles/ml. Consequently, the dilution of phosphoric acid mists with air is sometimes necessary. A stream of conditioned mists was allowed to pass through a measuring port of an Insitec PCSV-P laser optical particle counter. The size distribution of the mists was determined from the scattering light of a laser beam. In addition, a mist collector using the impactor and capillary action principles was constructed. The phosphoric acid mists were collected. The concentration of phosphoric acid in the mists was determined by an ion chromatography.

RESULTS AND DISCUSSIONS

The removal of NO from flue gas in the PhoSNOX process is based on the P_4-induced oxidation of NO to produce more soluble NO_2. The chemistry involved can be described by the following reactions:

$$P_4 + O_2 \xrightarrow{} P_4O + O \qquad (1)$$

$$P_4O \xrightarrow[n\,O_2]{} P_4O_{10} + m\,O \qquad (2)$$

$$O + O_2 \xrightarrow[M]{} O_3 \qquad (3)$$

$$NO + O_3 \longrightarrow NO_2 + O_2 \quad (4)$$

$$P_4O_{10} + 6\,H_2O \longrightarrow 4\,H_3PO_4 \quad (5)$$

P_4 reacts with O_2 to produce O and O_3 according to reaction (1) thru (3). Subsequently, O and O_3 oxidize NO to NO_2. NO_2 can be removed by scrubbing liquors through direct dissolution (6), by dissolution after forming N_2O_3 with NO (7), or by reaction with SO_3^{2-} or HSO_3^- ion (8).

$$2\,NO_2 + H_2O \longrightarrow NO_2^- + NO_3^- + 2\,H^+ \quad (6)$$

$$NO_2 + NO \quad N_2O_3 \longrightarrow 2\,NO_2^- + 2\,H^+ \quad (7)$$

$$NO_2 + SO_3^{2-}/HSO_3^- \longrightarrow NO_2^- + SO_3^-/HSO_3 \quad (8)$$

The presence of SO_3^{2-}/HSO_3^- at a concentration of greater than 1 mM in scrubbing liquor can cause[2] most of the NO_2 to react via (8) rather than (6). Consequently, most of the dissolved NO_2 is intially converted to HNO_2.

1. Removal Efficiency

The results of typical runs on the removal efficiency of NO are shown in Figure 2. Greater than 95 % NO removal efficiency were achieved at initial NO concentrations ranging from 58 to 610 ppm with an L/G of 16 liter/m^3 and a gas-droplet contact time of about 2 sec. The flue gas was under continuous flow conditions, whereas the P_4 reagent was under batch conditions with a limited amount of P_4 in the circulating liquors. The concentration of P_4 decreased with time, which resulted in the drop of NO removal efficiency. The removal efficiencies of SO_2 were greater than 95 % in these experiments, but were deleted from the figures to avoid confusion.

The NO removal efficiencies as a function of L/G and P_4 concentration in spray liquors are shown in Figure 3. The results were obtained from a set of experiments which were conducted by varying the flow rate of flue gas at a constant flow rate of recycling liquors. As a result, the contact time of the flue gas with the spray varied. The removal efficiency did not reach 90% until an L/G of 10 liter/m^3 with spray liquors of 0.5% P_4 concentration. The increase of P_4 concentration from 0.5% to 0.8% reduced the required L/G from 10 liter/m^3 to 8 liter/m^3 in order to achieve a 90% NO removal efficiency.

Because the diameter of the spray column is 4 inches, the droplets hit the wall a short distance after being sprayed. The liquor then flows down the wall of the column and exhibits poor contact with flue gas. Consequently, the mixing in the bench-scale system is not as effective as that in a commercial scale system at a given L/G. The consideration of the contact time of the droplets with flue gas may be more meaningful. Figure 4 shows a plot of the NO removal efficiencies as a function of contact time. The gas-droplet contact distance was estimated to be 2 ft. The contact time can be varied by changing the flow rate of the flue gas. The NO_x removal reached 90% efficiency with a contact time of 1.4 secs, which is less than that (2-5 secs) in a commercial system. However, it must be realized that the size of the droplets is smaller than those in a commercial system. Consequently, the mass transfer from gas to liquid is more effective in our bench absorber than in a commercial absorber. The utilization efficiency of P_4 can be expressed in terms of P/NO ratio. A P/NO ratio of as low as 0.6 has been achieved.

2. Byproducts Formation

The analysis[3,4] of scrubbing liquors from a bench-scale experiment revealed that less than 10% of the NO removed was converted to NO_3^-. The majority of NO removed was found to be in the form of nitrogen-sulfur compounds, which were produced as a result of the reaction of NO_2^- with HSO_3^-

$$NO_2^- + 2\,HSO_3^- \longrightarrow HON(SO_3)_2^{2-} + OH^- \quad (9)$$

$$HON(SO_3)_2^{2-} + H_2O \longrightarrow HOHNSO_3^- + HSO_4^- \quad (10)$$

$$HON(SO_3)_2^{2-} + HSO_3^- \longrightarrow N(SO_3)_3^{3-} + H_2O \quad (11)$$

$$N(SO_3)_3^{3-} + H_2O \longrightarrow HN(SO_3)_2^{2-} + HSO_4^- \quad (12)$$

$$HN(SO_3)_2^{2-} + H_2O \longrightarrow H_2NSO_3^- + HSO_4^- \quad (13)$$

These nitrogen-sulfur compounds can be converted to ammonium sulfate under extremely acidic conditions

$$H_2NSO_3^- + H^+ + H_2O \longrightarrow NH_4^+ + HSO_4^- \quad (14)$$

Alternative ways to remove the nitrogen-sulfur compounds from scrubbing liquors include the precipitation as potassium salts and the use of an electrodialysis technique. We have recently developed a new approach to suppress the formation of the aforementioned nitrogen-sulfur compounds. This approach involves the use of a sulfamic acid additive which can be produced from the reaction of urea and sulfuric acid. As a result of the addition of sulfamic acid in scrubbing liquors, the absorbed NO is converted to N_2.

$$HNO_2 + H_2NSO_3H \longrightarrow N_2 + HSO_4^- + H_2O + H^+ \qquad (15)$$

The majority of yellow phosphorus was oxidized by oxygen in flue gas to form P_4O_{10}, which subsequently absorbed moisture to form phosphoric acid mists. The analysis of spraying liquors by ion chromatography showed that only about 10% of these mists were absorbed into scrubbing liquors. The remaining 90% of mists stayed with the flue gas, as evidenced by its heavy white appearance. These mists must be removed from flue gas so that a valuable by-product, phosphoric acid, could be recovered and that the flue gas discharged from a stack could comply with opacity regulations.

3. Characterization of Phosphoric Acid Mists

The size distribution of the mists was determined in order to choose an appropriate collection device for the mists. Two different techniques, a cascade impactor and a laser optical particle counter, were employed to measure the size of mists for comparison. The results obtained from these two techniques are in good agreement. Table 1 shows that the geometric mean diameter of mists increases from 0.65 um to 1.1 um as the residence time extends from 0.7 sec to 11 sec. The size of the mists increases along with the residence time of the mists, which was attributed to the coagulation. However, a small decrease of temperature during the transit of the mists may result in the grow of the size from the condensation of moisture in spite of the temperature control along the pathway of the mists. The size distribution of the mists, in terms of mass frequency vs size, was measured by the optical particle counter. The size distribution of the mists peaked at 0.5 um, 0.9 um, and 1.2 um with a residence time of 0.7, 5.6, and 11.2 sec, respectively.

The concentration of phosphoric acid in the mists was about 10% by weight. This was determined by the collection of the mists with a sinter glass impactor. The solutions soaked in the sinter glass was sucked into a container through a capillary tube. The solutions collected was analyzed by an ion chromatography.

From the results of size and concentration measurements, the use of a submicron mist collector such as an Aerosep multi stage aerosol separation system may be necessary to recover the phosphoric acid mists. The residence time of phosphoric acid mists in a prescrubber or a scrubber is expected to be less than 5 sec. As a result, a substantial fraction of the mists is less than 1 um. In addition, the acid recovered has to be concentrated to about 75 wt % in order to produce a marketable byproducts.

4. Process Configuration

A conceptual process configuration of a wet PhoSNOX system with throw-away wastes may be derived as shown in Figure 5. An aqueous mixture of P_4 and an alkaline reagent such as limestone or soda ash may be sprayed in a scrubber. A mist collector is required to recover the phosphoric acid mists to comply with the opacity regulation and for by-product credit. An air-purged oxidation tank is installed to ensure the complete conversion of residual P_4 to phosphate ions before discharge. Besides the addition of a mist collector and an air-purged oxidation tank, this is a typical process configuration of a throw-away wet flue gas desulfurization system.

An alternative process configuration (Figure 6) may be derived where an aqueous mixture of P_4 and sulfamic acid is injected into a prescrubber or a section of the duct upstream from the scrubber where an alkaline solution/slurry is used to absorb acid gases. An Aerosep mist collector is installed between the prescrubber and the scrubber. A slip stream of liquor from a scrubber loop was fed into a prescrubber loop to ensure the conversion of absorbed NO_x to N_2.

5. Process Economic Projection

Pre-pilot plant economic projections for the PhoSNOX process have been made based on a preliminary conceptual process configuration with the following features:

- Injecting a phosphorus emulsion into an existing wet limestone scrubber, or injecting an aqueous mixture of yellow phosphorus and sulfamic acid into a new prescrubber
- Adding an "Aerosep" system downstream of the scrubber (or prescrubber) to capture and convert the P_2O_5 to phosphoric acid byproduct
- Installing necessary equipment to recover other phosphate byproducts
- Adding new fan capacity to compensate for the additional pressure drop
- Adding new equipment for phosphorus and byproducts storage
- Installing fire & safety protection equipment on phosphorus unloading, storage, and handling system.

The PhoSNOX process economics are compared with those reported in the literature for the Selective Catalytic Reduction (SCR) process, as shown in Table 2.

CONCLUSION

The PhoSNOX process is based on the addition of yellow phosphorus in wet flue gas desulfurization systems to allow simultaneous removal of SO_2 and NO_x from flue gas. The NO_x removal efficiency of PhoSNOX at 90+% could potentially be achieved at the actual conditions employed in wet FGD systems. Pre-pilot plant economic projections for the PhoSNOX process indicates that the capital installation costs for PhoSNOX are lower and operating costs are comparable when the process is compared with SCR.

REFERENCES

1. S.G. Chang, and D. K. Liu, "Removal of Nitrogen and Sulphur Oxides from Waste Gas Using a Phosphorus/Alkali Emulsion," Nature, 343, 151(1990).
2. D. Littlejohn, and S. G. Chang,"Modeling of the Chemistry of Wet Limestone Flue Gas Desulfurization Systems," Energy & Fuels, 5, 249 (1991).
3. D. Littlejohn, and S.G. Chang,"Determination of Nitrogen-Sulfur Compounds by Ion Chromatography," Anal. Chem.,58,158 (1986).
4. D. Littlejohn, and S.G. Chang,"Identification of Species in a Wet Flue Gas Desulfurization and Denitrification system by laser Raman Spectroscopy,"Environ. Sci. & Technol.,18, 305 (1984).

Table 1 Comparison of the Mean Diameters of Mists from Laser Scattering and Cascade Impactor Measurements

	Residence Time(sec)			
Methods	0.7	2.8	6.5	11.2
Laser	0.66 um	0.72 um	0.97 um	1.10 um
Impactor	0.67 um	0.67 um	0.83 um	

Table 2. Economics Comparisons: NO_x Removal Processes (500 MW, 300 ppm NO_x)

	Capital, $/kW	Levelized, mills/kWh
PhoSNOX (90% NO_x Removal; P/NO_x=0.5)		
W/O prescrubber	28	4.2
With prescrubber	43	4.7
SCR (80% NO_x Removal)		
EPRI (1991 NO_x Symposium Summary)	100	5 - 7
EPRI (1989 NO_x Symposium Summary)	78 - 101	4 - 9

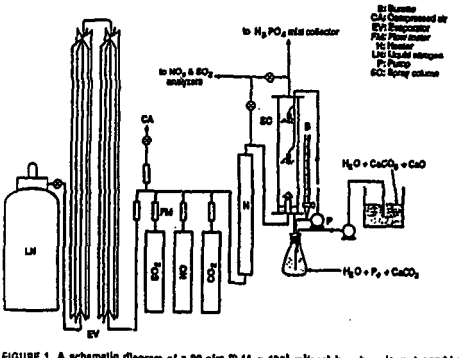

FIGURE 1. A schematic diagram of a 20 cfm [9.44 x 10^{-3} m^3/sec] bench-scale wet scrubber using yellow phosphorus and an alkaline for combined removal of SO_2 and NO, from a simulated flue gas.

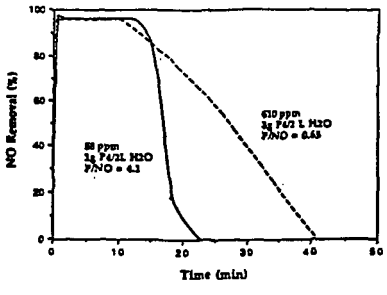

FIGURE 2. The removal efficiency of NO for NO concentrations of 58 and 610 ppm in a simulated flue gas.

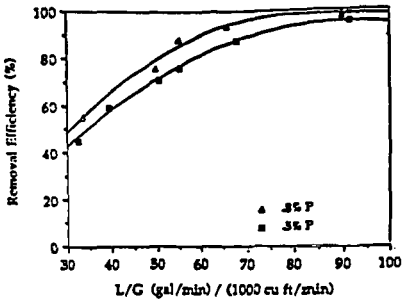

FIGURE 3. The removal efficiency of NO as a function of L/G [1 liter/m³ = 7.48 gal/1000 cu ft] with initial yellow phosphorus concentration of 0.5% and 0.8%.

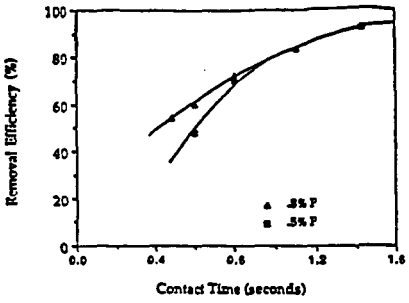

FIGURE 4. The removal efficiency of NO as a function of the contact time of spray droplets with a simulated flue gas.

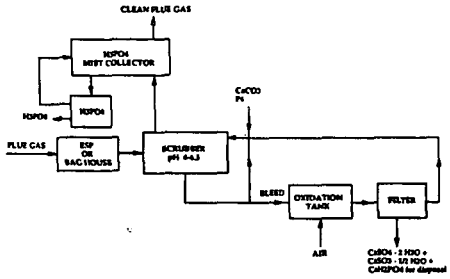

Figure 5 A conceptual process configuration of a wet PhoSNOX system with throw-away wastes

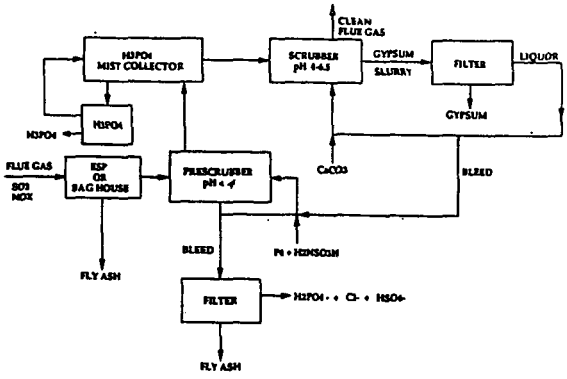

Figure 6 A conceptual process configuration of a wet PhoSNOX system with salable byproducts

ADVANCED IN-DUCT SORBENT INJECTION PROCESS FOR SO_2 CONTROL

J. A. Withum, W. A. Rosenhoover, M. R. Stouffer,
N. J. Delullis, D. C. McCoy
CONSOL Inc.
Research & Development
4000 Brownsville Road
Library, PA 15129

KEYWORDS: SO_2 Control; Hydrated Lime; Flue Gas Desulfurization; Sorbent Injection; Flue Gas Humidification

SUMMARY

This paper describes the status of development of an advanced duct-sorbent-injection process for the control of SO_2 emissions from coal-fired power plants. The technical objective of the project is to develop a low-capital-cost process capable of over 90% SO_2 removal as a retrofit option for compliance with the 1990 Clean Air Act Amendments. A complementary objective is to achieve sufficiently high sorbent utilization (60% with hydrated lime) so that levelized costs are lower than wet limestone scrubbing costs over a wide range of coal types and plant sizes.

The SO_2 removal and sorbent utilization objectives were achieved. The original performance targets of 90% SO_2 removal and 60% sorbent utilization were exceeded in 0.3 MWe pilot plant operations through a combination of equipment design improvements and sorbent recycle optimization. The 90% SO_2 removal target was achieved at sorbent utilizations of 70-75%. Up to 99% SO_2 removal was attained at 60% sorbent utilization. A simplified equipment design was tested and its operability was confirmed in pilot plant operation.

An interim economic evaluation was completed based on these results. Projected capital costs are approximately 40% lower than wet limestone scrubbing costs over the range of coal sulfur contents (1.5-3.5%) and plant sizes (160-500 MWe) evaluated. Levelized SO_2 control costs are competitive with wet limestone scrubbing over the range of cases studied. Potential design and operating improvements were identified which can reduce capital and levelized costs. These improvements will be evaluated in ongoing pilot plant development work. Current work also includes the development and testing of improved sorbents.

The advanced duct-sorbent-injection process (Advanced Coolside) involves flue gas humidification to the adiabatic saturation point using a contacting device which simultaneously removes fly ash from the flue gas. A sorbent (hydrated lime), injected into the highly humid flue gas downstream of the contactor, captures SO_2 before being removed in the existing particulate collector. The high humidity allows high SO_2 removal. High sorbent utilization is achieved by sorbent recycle. Greater recycle is possible than for previous duct-sorbent-injection processes because the fly ash is removed by the contactor prior to sorbent injection.

BACKGROUND

In-duct dry sorbent injection technology has been actively developed in the U.S. since the early 1980s. The performance of these processes has been well-established through the development of the Coolside process (CONSOL)[1-3] and the HALT process (Dravo)[4] and through the DOE duct injection technology development program.[5] These development efforts have included pilot-scale tests, proof-of-concept tests, and a full-scale utility demonstration. Established performance is in the range of 40-50% SO_2 removal at 2/1 Ca/S molar ratio and 20-25°F approach to adiabatic saturation temperature using hydrated lime as the sorbent. Additionally, the 105 MWe demonstration of the Coolside process at the Ohio Edison Edgewater Station[3] showed that an SO_2 removal of 70% can be attained by improving calcium hydroxide sorbent activity with sodium-based additive injection at a 0.2 Na/Ca molar ratio (~32% sorbent utilization).

Process performance data and economic analyses support the attractiveness of duct sorbent injection for site-specific applications.[6] However, the applicability as a compliance option for the Clean Air Act or other regulations can be expanded by improving SO_2 removals and sorbent utilizations. The performance targets for developing an advanced process (90% SO_2 removal and 60% sorbent utilization) represent a substantial improvement over previous technology.

The Advanced Coolside process is being developed using a 1000 acfm pilot plant.[7] The pilot plant was used in previous development of the Coolside process;[1,2] it was modified to include all elements of the Advanced Coolside process. Process development has focused on improving the design of the contactor and on improving sorbent utilization by optimizing sorbent recycle. A test program to investigate sorbent improvement was recently initiated. This report will discuss progress in these areas, results of the interim economic study and approaches for future process improvement.

DESCRIPTION OF ADVANCED COOLSIDE PROCESS

Figure 1 shows a schematic of the Advanced Coolside process. The process achieves higher SO_2 removal and sorbent utilization than previous duct sorbent injection processes by operating at a higher flue gas humidity and by more fully exploiting the potential of sorbent recycle. The key to the process is a gas/liquid contacting device downstream of the air preheater. The contactor serves two purposes: to nearly saturate the flue gas with water, and to remove most of the coal fly ash from the flue gas. The sorbent is injected downstream of the contactor into the highly humid flue gas. Hydrated lime is very

active for SO_2 capture near the saturation point. Because the flue gas is already humidified prior to sorbent injection, there is no strict residence time requirement for droplet evaporation. SO_2 is removed in the duct and by the sorbent collected in the existing ESP or baghouse. The heat of reaction between SO_2 and hydrated lime raises the temperature of the flue gas by roughly 9°F for each 1000 ppm of SO_2 removed. Therefore, it is possible to operate the particulate collector at a practical approach to saturation without flue gas reheat. However, because hydrated lime activity is highly sensitive to the approach to saturation, this reaction heat effect can also act as a limiting mechanism for SO_2 capture.

The spent sorbent is captured by the existing particulate collector as a dry powder. It can be disposed of with the fly ash or separately. Sorbent recycle is an integral component of the Advanced Coolside process. Recycle sorbent is quite active for SO_2 capture at high humidity. The potential for recycle is increased because fly ash is removed separately before sorbent injection. Furthermore, recycle sorbent performance can be improved by a simple physical pre-treatment step prior to re-injection; the nature of this pre-treatment step is currently a proprietary feature of the process.

Design optimization has focused on the flue gas/water contactor. For the initial pilot plant testing the contacting device was a Waterloo scrubber.[8] This is a commercially available device, marketed by Turbotak, Inc., and used primarily for removal of submicron particles. The Waterloo scrubber consists of a conditioning zone, a centrifugal fan and a mist eliminator, and uses two-fluid nozzles to finely atomize water sprays at a liquid/gas ratio of about 1 gal/1000 acf.

DISCUSSION

Recycle Optimization. The improvement in desulfurization performance which allowed project performance targets to be exceeded resulted primarily from recycle optimization. By more fully exploiting recycle, sorbent utilization efficiencies of 70-75% were attained, while maintaining SO_2 removal around 90%. Also, high SO_2 removals ranging from 90% to over 99% were attained, while maintaining sorbent utilization of 60%.

Recycle optimization tests were conducted in the 1000 acfm pilot plant in a semi-continuous manner. Spent sorbent was removed frequently from the pilot baghouse. A portion of the material was discarded and the remainder, after pretreatment, was returned in a batch to the recycle feeder. Test duration was sufficiently long to assure that steady-state continuous recycle was simulated closely (typically 20-70 hr).

Tables 1 and 2 list process conditions and results for pilot recycle optimization tests. Tests 1 through 4 (Table 1) were conducted with reheat before the baghouse (to a 25°F approach) to minimize baghouse SO_2 removal. The purpose was to simulate conditions in a retrofit application with an existing ESP. In this case, SO_2 removal in the ESP would be limited by gas phase mass transfer. Based on literature information and on theoretical calculations, an ESP removal of 30% of the SO_2 remaining in the ESP inlet gas is a reasonable assumption. As shown in Table 1, SO_2 removal in the baghouse with reheat averaged 5% (absolute). Tests 5-9 (Table 2) were conducted with no baghouse reheat. The 9 to 12°F baghouse approach temperature was a result of the flue gas temperature rise from the heat of reaction. In these tests SO_2 removal in the baghouse was greater than with reheat, although the large majority of SO_2 was still removed in the duct.

The recycle test results indicate that for systems with an existing ESP, 90% SO_2 removal can be achieved at sorbent utilizations of 70-75%, substantially higher than the original target of 60% utilization. For example, with a fresh Ca/S mol ratio of 1.2, duct and system SO_2 removals were 87% and 90%, respectively (Test 2, Table 1).

The results also indicate that high efficiency SO_2 removal can be attained in systems with a baghouse operated at close approach. For example, 99% SO_2 removal was attained at 61% sorbent utilization (Test 9, Table 2). In this test most of the SO_2 removal (88%) occurred in the duct. The capability to achieve very high SO_2 removal may be attractive to new units using a baghouse for fly ash collection.

In the recycle tests in Tables 1 and 2, recycle ratios ranged from 3.3 to 6.9 lb/lb fresh lime. Relatively high recycle ratios are possible because fly ash is removed upstream of sorbent injection. Total dust loading ranged from 9.5 to 14.5 gr/scf. Pilot testing indicated that recycle sorbent particles tended to agglomerate during handling, pretreatment and reaction; this could improve the ability of an existing ESP to handle higher dust loadings.

As shown in Tables 1 and 2, the recycle tests were relatively long-term. With one exception, operating durations ranged from 21 to 115 hr. This allowed process operability to be evaluated. It also provides added confidence in data reliability.

Data reliability also was confirmed by comparing utilizations based on gas analysis with those based on solids analysis. As shown in Tables 1 and 2, utilizations by the two independent methods agreed very well. This confirms the accuracy of process performance data; it also confirms that steady-state continuous recycle conditions were established. In addition, in-duct SO_2 removal data for selected run periods were confirmed by manual flue gas sampling using EPA Method 6.

Design Optimization. A major portion of the process development is devoted to contactor simplification. The contactor is a key capital cost component, and the contacting device initially tested was designed for more stringent applications (i.e., submicron particulate control) than required for Advanced Coolside. Because the process is applied upstream of an existing particulate collector, some fly ash slippage through the contactor is acceptable. It is only necessary to remove a large portion of the particulate mass (ca. 90%) to avoid recycling much of the inert fly ash. Approaches to reduce the capital and operating

cost of the contactor included eliminating the fan, an integral component of the original Waterloo scrubber system, and redesigning the contactor to reduce water and atomization air requirements.

Preliminary pilot plant studies indicated that these approaches are feasible. Tests were conducted using the original Waterloo scrubber system with and without its centrifugal fan under a wide range of atomizing air pressures and water flow rates. The test results (Figure 2) indicated that high flue gas relative humidities can be achieved with or without the fan, as long as sufficient water droplet surface area is generated in the contactor. The test results also showed that the atomization energy can be reduced to below typical operating conditions (40-45 psig) with a relatively minor effect on flue gas humidity. Particulate removal tests indicated that removal efficiency was not sensitive to the nozzle operating conditions over the ranges tested and that the scrubber fan was not needed to achieve fly ash removal greater than 90 wt %. These results indicate that there was flexibility for design and operating modifications.

Based on the tests using the original contactor, a mechanically simpler contactor was designed by Turbotak Inc. (Figure 3). The new contactor consists of a spray chamber and a downstream mist eliminator. Most of the particles and water droplets are removed in the spray chamber. The mist eliminator removes remaining droplets from the flue gas. The Waterloo scrubber fan was eliminated, significantly reducing the cost of the contactor.

Tests were performed which verified the humidification performance, particulate collection efficiency, and operability of the simplified contactor. Optimization tests were conducted to reduce atomization air pressure and flow and water flow relative to the design conditions of Turbotak. Table 3 shows the result of using the alternative operating conditions identified in these tests. Water and air flow requirements were reduced by about half. The air pressure requirement was reduced from 45-50 to ~30 psig, while maintaining humidification (>95% relative humidity) and fly ash removal efficiency (> ca. 90%). These alternative operating conditions will result in lower operating and capital costs.

Operability Observations. Pilot plant operating experience in tests up to 115 hr in duration is a positive indication of the operability and retrofit potential of the Advanced Coolside process. Although the pilot plant is not of sufficient scale to make a complete assessment of process operability, observations of pilot plant operation provide initial information on key operability issues.

The contactor operability was simplified by the elimination of the fan. The mist eliminator was washed periodically to maintain contactor pressure drop at about 1.5 inches of H_2O.

Accumulation of solids on the duct walls was not an operating problem, even at very close approach to saturation and with different duct configurations having short straight-run residence times (<0.5 sec) and numerous changes in flow direction. There was generally a light surface coating of dry solids. At bends, there was somewhat more accumulation. The amount of solids on the duct surface tended to reach a steady value after 10 to 30 hr of operation, after which the rate of accumulation approached zero. The solids were loose and easily removed.

No major problems were encountered in preparing, handling and feeding the recycle sorbent. Operability of the pneumatic transport system was similar to that with hydrated lime. Operability of the recycle handling system was observed to deteriorate at very high sorbent utilization (>70%). This was alleviated by adding the fresh lime to the recycle material during pre-treatment and co-injecting the sorbents.

Baghouse operability was good at the close approaches to adiabatic saturation (down to 10°F) investigated in this program. The material did have a tendency to compact under compression at the lowest baghouse approach temperature, an important consideration for a larger scale design.

Sorbent Optimization. Sorbent improvement can increase the attractiveness of the Advanced Coolside process in several ways. Increasing sorbent utilization reduces sorbent usage and waste disposal requirements. Increasing sorbent activity can reduce the required level of sorbent recycle and could increase the applicability of the process for high SO_2 removal levels. Finally, the results of sorbent studies could allow use of lower cost sorbents by reducing process sensitivity to sorbent source.

Pilot plant tests reported previously in this paper were all conducted with a single commercial hydrated lime. A sorbent optimization test program was recently begun. The program includes work in three areas: a lime hydration study, evaluation of alternate sorbents, and evaluation of additive enhancement.

The objectives of the lime hydration study are to determine the effect of hydration variables on the properties of hydrated lime and to determine the effect of lime properties on desulfurization performance. The hydration study is being conducted in cooperation with Dravo Lime Co. using their continuous pilot hydrator. Hydration variables being investigated in a statistical experimental design include the following: quicklime source, quicklime grind size, hydration water temperature, residual H_2O in the product, and hydrator residence time. Hydrated limes will be characterized for chemical composition and physical properties such as particle size, surface area, and pore size. Desulfurization performance will be measured in laboratory reactors and in the pilot plant.

Evaluation of alternate sorbents will include testing of different commercial hydrated limes and testing of other sorbents, for example, specially prepared high surface area hydrated limes. Recycle tests were conducted for two commercial hydrated limes. In these tests at 1.2 Ca/S mol ratio, system SO_2 removals (with baghouse reheat to simulate ESP removal) were 90% and 86% for the hydrated limes with surface areas of 22 and 14 m^2/g, respectively. Also, once-through screening tests of different commercial hydrated limes from different geographic regions and with varying surface areas showed only small differences in SO_2 removals. These results suggest that process performance is relatively insensitive to

surface area and to commercial lime source. This may be an economic advantage, allowing use of the lowest cost sorbent available.

Previous laboratory studies[7] simulating Advanced Coolside process conditions indicated that sodium-based additives can substantially increase the utilization of hydrated lime (by over 20% absolute). In the current test program, different approaches for additive promotion will be investigated, including addition to lime during hydration. Based on previous lab studies and literature information, additives to be evaluated include Na_2CO_3, NaCl, and $CaCl_2$. Chloride additives are of interest because they could be generated by neutralization of contactor recycle water. One pilot plant test was conducted with NaCl promotion. Results are encouraging, indicating that sorbent utilization can be increased to 80-85% using very small amounts of additive — 0.025 Na/S mol/mol, about 1/15 of that employed in the conventional Coolside process.[1-3] Further testing is under way using different additives and additive dosages, and varying process conditions.

Process Economics. An interim process economic study was completed based on current process performance data with a commercial hydrated lime and a conceptual process design. The objectives for this study were to confirm the potential economic advantages of the Advanced Coolside process and to identify priorities for further process development. A final economic study will be conducted at the conclusion of the pilot-scale development program.

The economic study compared costs of Advanced Coolside with limestone wet scrubbing. Economic assumptions (Table 4) were selected to assure comparison on an equivalent basis. The limestone wet FGD costs are based on a design which includes forced oxidation and a single absorber module. Both processes were evaluated for 90% SO_2 removal efficiency, an assumed capital life of 30 years and using the same retrofit factors. The analysis was based on an "nth" plant design philosophy, using an 18% contingency for each process.

The economic study confirmed a substantial capital cost advantage for the Advanced Coolside process. Figure 4 shows that for a 2.5% sulfur coal the capital cost was about 40% less than forced oxidation limestone scrubbing, over the 150-500 MWe range of plant sizes studied. The relative difference in capital cost was about the same for 1.5 and 3.5% sulfur coals. The lower capital cost can be important to utilities in making compliance decisions because it reduces financial and regulatory risk.

The economic study quantified the potential SO_2 control cost advantages of the Advanced Coolside process. Figure 5 shows that the process has a lower levelized cost ($/ton SO_2 removed) than limestone wet FGD over a wide range of coal sulfur contents and plant sizes. The cost differential ranged from 21% for 1.5% sulfur coal and a 150 MWe plant, to 11% for 2.5% sulfur and 250 MWe, to breakeven for 3.5% sulfur and 500 MWe.

The interim study also indicated that there is potential for further improvement of the Advanced Coolside process and identified areas for improvement with the greatest potential impact on economics, including reduction in sorbent cost and reduction in equipment capital cost for certain process systems. Areas for equipment cost reduction include further contactor optimization and improvement in other systems on which optimization studies have not yet focused (e.g., recycle handling, waste handling, and flue gas handling). The goal of further development is to establish at least a 20% levelized cost advantage over wet FGD over a wide range of compliance situations. This would make it more attractive for utilities to employ a newer, less established technology.

FUTURE WORK

Based on the process economic study, the focus of future process development will be to increase the cost advantage of Advanced Coolside over commercial technology through equipment design optimization and sorbent improvement. For the economic study, Turbotak, Inc. developed preliminary full-scale designs for the simplified contactor based on the test results with the original contactor. The results of pilot tests using the new contactor will be used by Turbotak to develop a commercial design to further reduce costs. Equipment design optimization efforts will be expanded to look at other systems with potential impact on process capital cost, as identified in the economic study. The sorbent improvement work under way will continue as described above. The goals are to reduce sorbent usage and to allow use of lower cost sorbent sources. Another area for future investigation is air toxics control, particularly that of mercury. A literature analysis under way suggests that the Advanced Coolside process has potential for Hg reduction. The capability for air toxics control would provide an additional incentive to use this technology for SO_2 compliance.

ACKNOWLEDGMENT

This work was conducted under partial sponsorship of the U.S. Department of Energy Contract DE-AC22-91PC90360. The authors are grateful to C. J. Drummond, T. D. Brown and others at DOE/PETC for their support and encouragement of this project.

REFERENCES

1. Yoon, H.; Stouffer, M. R.; Rosenhoover, W. A.; Withum, J. A.; Burke, F. P. "Pilot Process Variable Study of Coolside Desulfurization", *Environ. Progress* **1988**, 7(2), 104-11.
2. Stouffer, M. R.; Yoon, H.; Burke, F. P. "An Investigation of the Mechanisms of Flue Gas Desulfurization by In-Duct Dry Sorbent Injection", *I&EC Research* **1989**, 28(1), 20.
3. Withum, J. A.; Yoon, H.; Burke, F. P.; Statnick, R. M. "Coolside Desulfurization Demonstration at Ohio Edison Edgewater Power Station", *ACS Div. Fuel Chem. Preprints* **1990**, 35(4), 1463-72.

4. Babu, M.; College, J.; Forsythe, R. C,; Herbert, R.; Kanary, D. A.; Kerivan, D.; Lee, K. "5 MW Toronto HALT Pilot Plant", Proceedings, 4th DOE-PETC Contractors' Meeting, Pittsburgh, PA, August 1988.
5. Felix, L. G.; Gooch, J. P.; Merritt, R. L.; Klett, M. G.; Hunt, J. E.; Demian, A. G. "Scale-Up Tests and Supporting Research for the Development of Duct Injection Technology", Presented at the 1991 SO_2 Control Symposium, Washington, DC, December 1991.
6. Nolan, P. S.; McCoy, D. C.; Statnick, R. M.; Stouffer, M. R.; Yoon, H. "Economic Comparison of Coolside Sorbent Injection and Wet Limestone FGD Processes", Presented at the 1991 SO_2 Control Symposium, Washington, DC, December 1991.
7. Stouffer, M. R.; Rosenhoover, W. A.; Withum, J. A. "Advanced Coolside Desulfurization Process", Presented at the 1992 Summer National Meeting of the American Institute of Chemical Engineers, Minneapolis, MN, August 9-12, 1992.
8. Spink, D. R. "Handling Mists and Dusts", *CHEMTECH* 1988, 364-8.

TABLE 1. Advanced Coolside Pilot Plant Recycle Tests with Flue Gas Reheat Prior to the Baghouse.

Test	1	2	3	4
Test Duration, hr	36	115	13	73
Process Conditions				
Fresh Ca/S, mol	1.4	1.2	1.5	1.2
Recycle Ratio, lb/lb fresh lime	4.5	6.9	4.4	6.7
Recycle Pretreatment	Yes	Yes	Yes	Yes
Baghouse Approach Temp., °F	23	23	24	22
Hydrated Lime	A	A	A	B
Process Performance				
SO_2 Removal, %, In-Duct	83	67	84	80
System	90	90	90	86
Baghouse	7	3	6	6
Sorbent Utilization, %, By Gas Analysis	63	75	60	70
By Solid Analysis	63	70	59	71

Common Condition: SO_2 Content: 1500 ppm

TABLE 2. Advanced Coolside Pilot Plant Recycle Tests with No Flue Gas Reheat Prior to the Baghouse.

Test	5	6	7	8	9
Test Duration, hr	40	28	21	25	23
Process Conditions					
Fresh Ca/S, mol	1.2	1.5	1.2	1.6	1.6
Recycle Ratio, lb/lb fresh lime	3.3	3.5	4.9	3.9	3.6
Recycle Pretreatment	Yes	Yee	Yes	Yee	Yes
Baghouse Approach Temp., °F	9	12	9	11	12
Hydrated Lime	A	A	A	A	A
Process Performance					
SO_2 Removal, %, In-Duct	60	70	61	91	88
System	84	90	88	97	99
Baghouse	24	20	7	6	11
Sorbent Utilization, %, By Gas Analysis	67	61	71	80	61
By Solid Analysis	68	63	68	56	61

Common Condition: SO_2 Content: 1500 ppm

TABLE 3. Optimization of Contactor Operating Conditions.

	Base Design	Alternative
Conditions		
Nozzle Water Flow	1.13 gpm/1000 acfm	0.6 gpm/1000 acfm
Nozzle Air Pressure	45-50 psig	30 psig
Nozzle Air Flow	17 scfm/1000 acfm	9 scfm/1000 acfm
Performance		
Exit Humidity	>98%	>98%
Fly Ash Collection	>95%	~95%

TABLE 4. Key Assumptions of Interim Process Economic Study.

	Advanced Coolside	Forced Oxidation Wet FGD
Delivered Sorbent Cost	$60/ton, 7% inerts (hydrated lime)	$15/ton (limestone)
Waste Disposal Cost	$6.50/ton	$6.50/ton
SO_2 Removal	90%	90%
Capacity Factor	65%	65%
Capital Life	30 years	30 years
Retrofit Factor	Medium (1.22-1.34)	Medium
Location Factor	1.06	1.06
Design Philosophy	"nth" plant, 18% capital contingency	"nth" plant, 18% capital contingency
Sparing	Auxillary equip. only, no major equip.	Auxillary equip. only, no major equip.
Indirect Costs	37.2% of direct	37.2% of direct

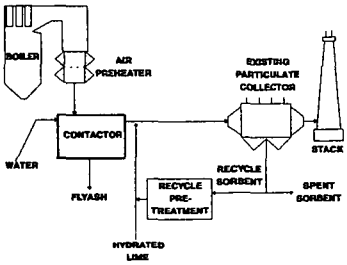

Figure 1. Advanced Coolside Process Schematic.

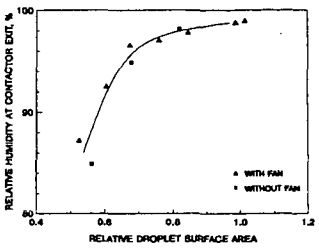

Figure 2. Initial Pilot Test Data for Contactor Simplification.

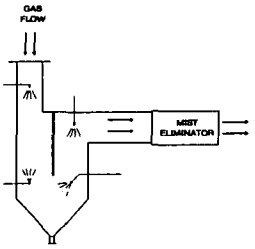

Figure 3. Simplified Contactor Design.

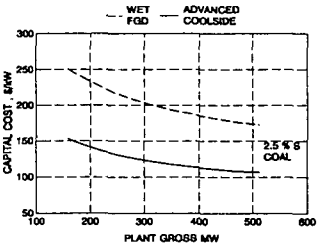

Figure 4. Comparison of Capital Costs for Advanced Coolside and Wet Limestone Forced Oxidation FGD at 2.5% Coal Sulfur Content and Varying Plant Sizes.

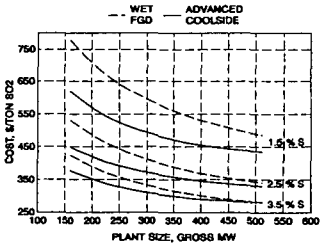

Figure 5. Comparison of Levelized SO_2 Control Costs for Advanced Coolside and Wet Limestone Forced Oxidation FGD as a Function of Coal Sulfur Content and Plant Size.